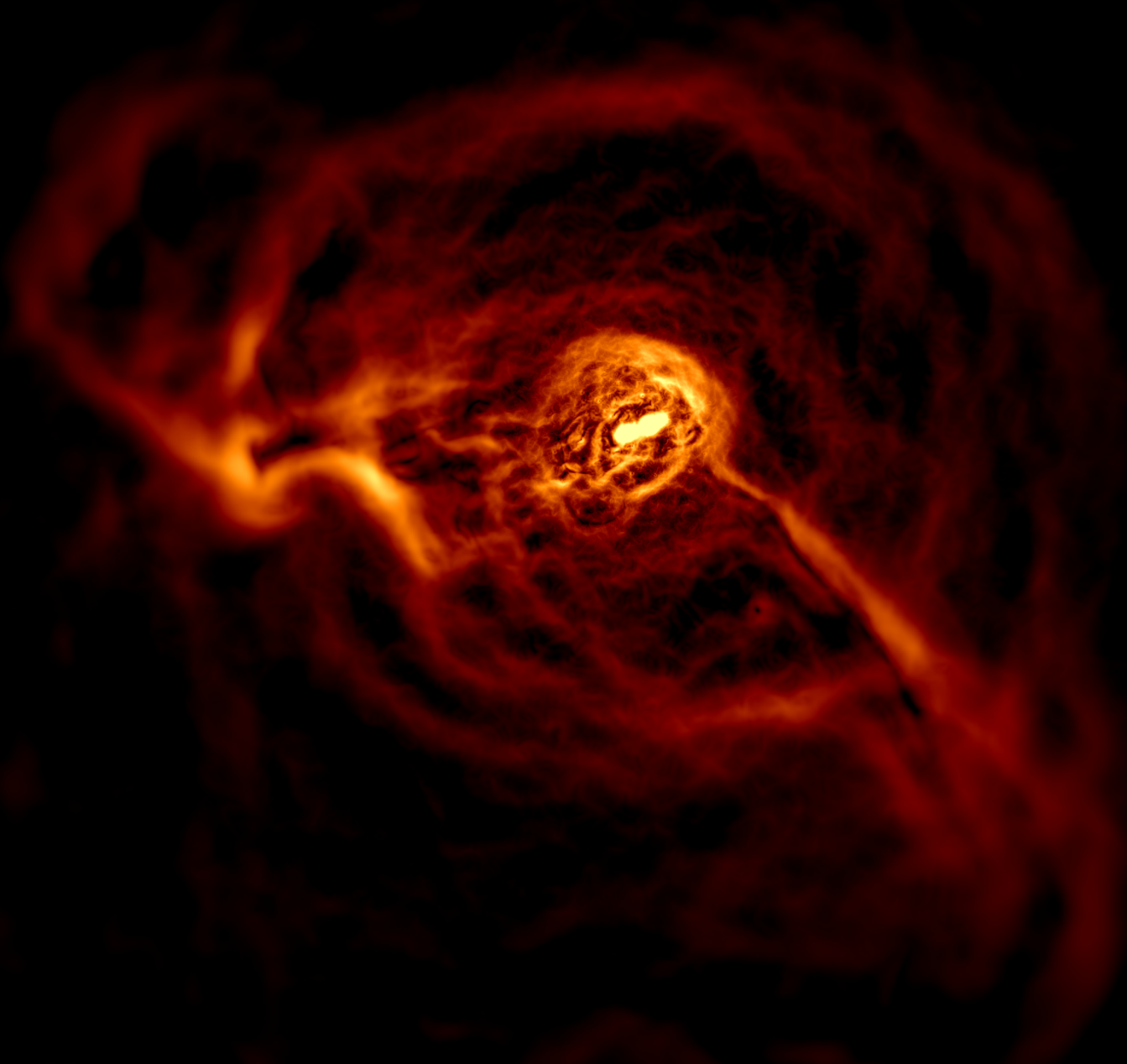


Chandra News

Issue 25 Spring 2018

Edge Detection Gives Chandra a Sharper View of Cluster Astrophysics

Jeremy Sanders, Stephen Walker, John ZuHone, Elena Bellomi



Contents

Edge Detection Gives <i>Chandra</i> a Sharper View of Cluster Astrophysics	1
Director's Log, <i>Chandra</i> Date: 634348806	7
Project Scientist's Report	10
Project Manager's Report	11
ACIS Update	12
HRC Update	13
HETG Update	14
LETG Update	17
Chandra-Related Meetings and Important Dates	19
Brent Williams (1974-2017)	20
<i>Chandra</i> Calibration Update	21
<i>Chandra</i> Source Catalog	22
From <i>Chandra</i> to <i>Lynx</i> : A Summary of the Conference	23
CIAO in India.	26
The Einstein Postdoctoral Fellowship Program: Morphing and Merging	28
Visualizing and Using the Global <i>Chandra</i> Footprint.	29
Data-Driven VR/AR 3D Models: Walking Among the Stars	30
The Results of the Cycle 19 Peer Review	32
2017 Press Releases	36
The <i>Chandra</i> Bibliography	37
Useful <i>Chandra</i> Web Addresses	39
<i>Chandra</i> Users' Committee Membership List	40
<i>Chandra</i> Science Workshop on Accretion	41

The *Chandra* Newsletter appears once a year and is edited by Rodolfo Montez Jr., with editorial assistance and layout by Tara Gokas. We welcome contributions from readers. Comments on the newsletter, or corrections and additions to the hardcopy mailing list should be sent to: chandranews@cfa.harvard.edu.

Follow the *Chandra* Director's Office on *Facebook*, *Google+* and *Twitter* (@ChandraCDO).

Edge Detection Gives *Chandra* a Sharper View of Cluster Astrophysics

Jeremy Sanders, Stephen Walker,
John ZuHone, and Elena Bellomi

Introduction

The X-ray surface brightness of galaxy clusters peaks steeply like a mountain, and like a mountain it can be very hard to see the interesting features on the slopes from far away. Although some clusters can be very pointed, some slightly flat-topped and some with more than one peak because they are merging together, they all have large dynamical ranges in surface brightness from the faint outskirts to the bright central region. The intracluster medium, which is the hot atmosphere that fills clusters and accounts for most of their baryons, generates the X-ray emission. The X-ray emission is sensitive to the density-squared of this material, meaning the X-ray brightness grows steeply as the density increases towards the center.

Because of this sensitivity to density, studying the X-ray emission provides vital clues to understand what physical processes are taking place in clusters. Feedback by active galactic nuclei, sloshing of gas in the potential well of the system, and mergers all affect the gas density. The issue is that the scale of these variations is often relatively small compared to the peak as a whole. While major mergers, like the Bullet cluster, are easy to see directly in an X-ray image, simulations of clusters show we should expect a lot of structure on small scales (a few kpc) in all clusters, particularly if turbulence or fluid instabilities are present. This problem is compounded when viewing images of clusters on media with limited dynamic range.

Structure-Finding Methods for Imaging

A common way to remove the peak and see the interesting edges, filaments, cavities or ripples is to model the cluster emission, then subtract or divide the X-ray image or surface brightness profile by the model. This often works well, but real clusters are not spherical beta models (note that a beta model is a common parameterization for the X-ray surface brightness with a flat core and a powerlaw at larger radii, although this is not what the average cluster looks like—see Sanders et al. 2018). The model can either be too crude to account for most of the cluster emission, or inappropriate modeling can introduce structure that is not present and can also remove interesting features by over-modeling.

After the launch of *Chandra* with its high spatial resolution imaging, the problem became acute. This led to the use of image processing techniques, such as unsharp masking, being applied to *Chandra* data. Unsharp masking has a long

history of being applied to astronomical data. David Malin, in particular, is famous for applying it to photographic astronomical images (Malin & Zealey 1979). When used in X-ray astronomy, the typical observer smooths their image by a Gaussian with a particular length scale and subtracts or divides this from the image smoothed by a smaller or no Gaussian. In this way, large scale fluctuations are removed to reveal the small scale features in the data. This technique has, for example, uncovered the ripple-like structures in the Perseus cluster (Fabian et al. 2003). Unsharp masking is a simple but powerful technique and is well suited for detecting compact single-scale features. It does not work as well for elongated linear structures.

Other forms of structure detection in clusters have included wavelet decomposition, which decomposes images into various scales (e.g., Grebenev et al. 1995). If the emission you are interested in has a dominating scale, wavelets are a good choice to search for such structure. We have also investigated filtering out large scales in the spatial frequency domain with success (Sanders & Fabian 2008), although care has to be taken that aliasing and the frequency wings of bright sources do not introduce spurious features.

The Gaussian Gradient Magnitude (GGM) Filter

Working on a deep *Chandra* observation of the Centaurus cluster (Sanders et al. 2016a), it was suggested by Katherine Blundell to try out the Sobel filter on our high quality X-ray data, to highlight the edges in the surface brightness. The Sobel filter or operator is a simple convolution with a 3×3 matrix which measures the pixel-scale gradient in the image it is applied to in one direction. The Sobel filter has been used in radio astronomy previously to highlight edges in jets (e.g., Laing et al. 2013). In addition, edge filters have also been applied when analyzing cluster simulations (Roediger et al. 2013), but we are not aware of applications on X-ray data. Edge detection also has a long history in computer vision applications. We discovered with further experimentation that a more advanced version of a gradient filter, the Gaussian Gradient Magnitude (GGM), was an excellent tool for revealing edges in cluster images. In this filter, the image is convolved with a function which is the gradient of a Gaussian in either the X or Y directions with a particular size scale, measuring the gradients on this scale. The two gradient images can then be used to compute the gradient magnitude for that scale.

Measuring surface brightness gradients is optimal for cluster studies because many of the physical processes in clusters create edges or shells which lead to strong gradients. For example, a cold front is a discontinuity in temperature and density thought to be generated by sloshing of the intracluster medium in the potential well of a cluster caused by an interloper which disturbs that well (Markevitch & Vikhlinin 2007). Another example is a shock, perhaps generated by a merger or AGN outburst, that can be seen via

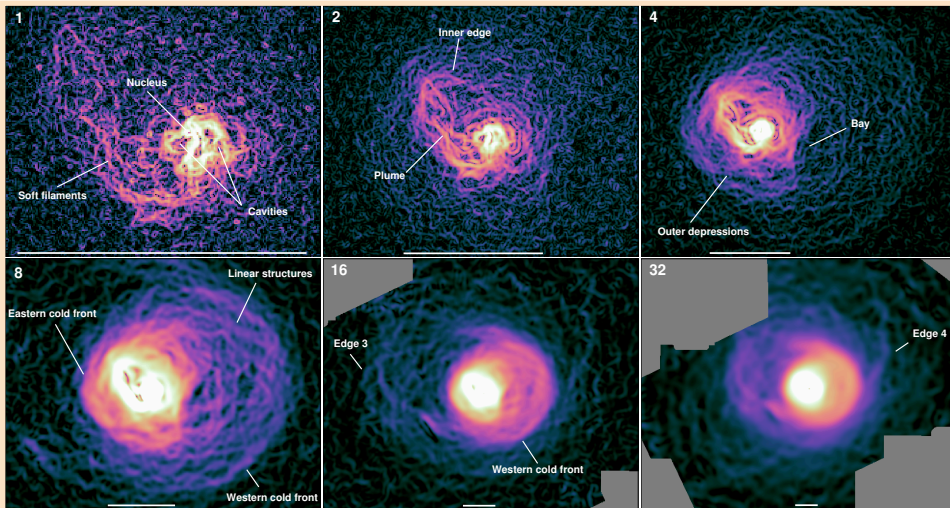


Figure 1: Images of the Centaurus cluster with the gradient measured on scales increasing by a factor of two, in units of one $\frac{1}{2}$ arcsec pixel (north is up, and east is left). The white bars show 20 kpc in each panel. Adapted from Sanders et al. (2016a).

its density jump. *Chandra* has revealed that cavities, filled with relativistic bubbles generated by the central AGN, are an almost ubiquitous feature of clusters with short central cooling times.

We applied the GGM technique to very deep *Chandra* X-ray images of the Centaurus cluster. Centaurus is a nearby ($z \sim 0.01$) X-ray bright galaxy cluster. Several physical processes are occurring within the cluster; the main subcluster is merging with another 200 kpc away, the core shows clear evidence for episodic AGN outbursts and contains some of the clearest examples of cold fronts in the universe.

Figure 1 shows filtered images of the Centaurus cluster, with filtering scales increasing by factors of two, after masking out point sources. In the image, high-gradient regions, or edges, are represented by bright colors while dark colors show the low-gradient regions. There are two cavities which lie either side of the nucleus in the center and in the smallest-scale image we see their sharp edges. These cavities are filled by AGN-outburst generated bubbles of relativistic plasma seen by its radio emission. These bubbles are weakly shocking their surroundings when examined with detailed spatially resolved spectroscopy. There is a plume of soft filamentary emission, first seen in early *Chandra* observations of this object (Sanders & Fabian 2002), that we suggest is caused by cooler material lifted out from the core of the cluster in the wake of a buoyantly rising bubble of plasma, whose edge seen in Panel “2” (labeled “Inner edge”). There is also low frequency radio emission seen inside this region, supporting this origin (Figure 3 bottom right). We also see evidence for a number of edges associated with depressions, labeled “Outer depressions”. We interpret these as caused by bubbles from old episodes of AGN outbursts, as there is also low frequency radio emission associated with them in the opposite direction of the plume. In panel “8” there are a number of

linear structures. We hypothesize these could be sound waves generated by outbursts of the AGN. In that case their wavelength implies a period of around 6 Myr. Alternative explanations include Kelvin-Helmholtz instabilities (KHI) or magnetic field structures. On larger scales are the two cold fronts, “Eastern cold front”, in panel “8” and one the western one at larger radius (“Western cold front” in panels “8” and “16”). There are also two further possible cold fronts, labeled Edge 3 and Edge 4.

Not all of the structure revealed by the GGM filtering technique in the images is real. Poisson noise in these filtered images has a peculiar “wormy” nature, so care should be taken that the features are real and not due to noise (see “Assessing the significance of features” on page 3).

For visual purposes it is useful to combine together images filtered on different scales. This is important in the outskirts of the cluster where the count density is too low to measure the gradient. We developed a simple technique to add images filtered on different scales using a radial weighting function. With the aid of a graphical user interface we can interactively adjust the weighting to highlight the significant edges in the image while reducing the noise-related artifacts from low count density regions.

Figure 2 shows our combined filtered image of M87 in the center of the Virgo cluster, combining 1Ms of *Chandra*

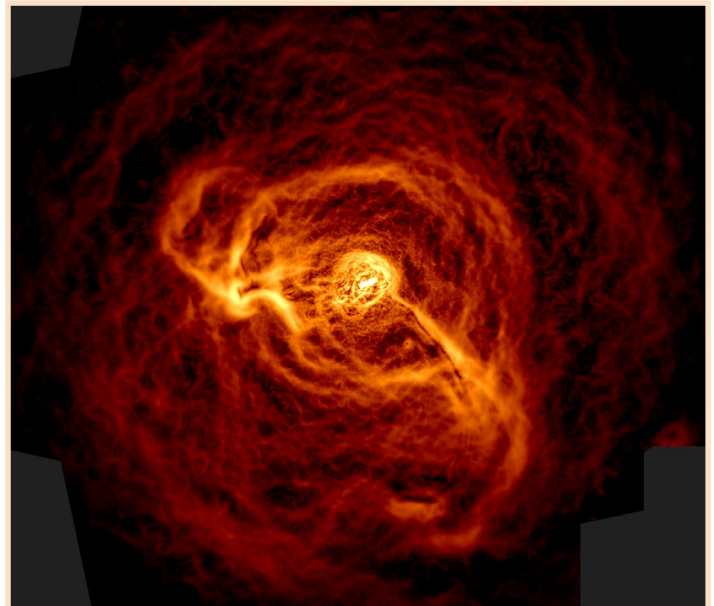


Figure 2: Multi-scale filtered X-ray image of M87 in the center of the Virgo cluster. Created by radially combining filtered images with scales of 1 to 32 $\frac{1}{2}$ arcsec pixels. The image measures 80 kpc across.

data. The combined filtered image allows us to display a great deal of structure in a single image. The image covers the jet in the central region (Marshall et al. 2002), the surrounding cavities generated by a cocoon of relativistic plasma (Young et al. 2002), the well known arms of soft X-ray emission interacting with the radio source (Forman et al. 2007), and the circular structure of ~ 14 kpc radius from a weak shock generated an outburst of the central AGN (Forman et al. 2007).

Gradient filtering is particularly well-suited for uncovering edges in imaging of clusters, while unsharp masking is perhaps a better choice to identify spatially compact clumps or cavities. Many of the structures in clusters, for example cold fronts, cavity edges, shocks, are edge-like in nature, so gradient filtering is an excellent choice to find them.

Science Discoveries: A Kelvin-Helmholtz Instability (KHI) in the Sloshing Cold Front of the Perseus Cluster

Deep *Chandra* observations of nearby galaxy clusters, (namely the Perseus cluster, the Centaurus cluster, and Abell 1795) have revealed unusual concave surface brightness edges referred to as “bays”. Walker et al. (2017) explored the various possible formation scenarios for these bays, by combining X-ray and deep radio observations and comparing these observations to simulations of gas sloshing. We found that these bays cannot be simply explained by AGN feedback activity or standard convex sloshing cold fronts (Figure 3).

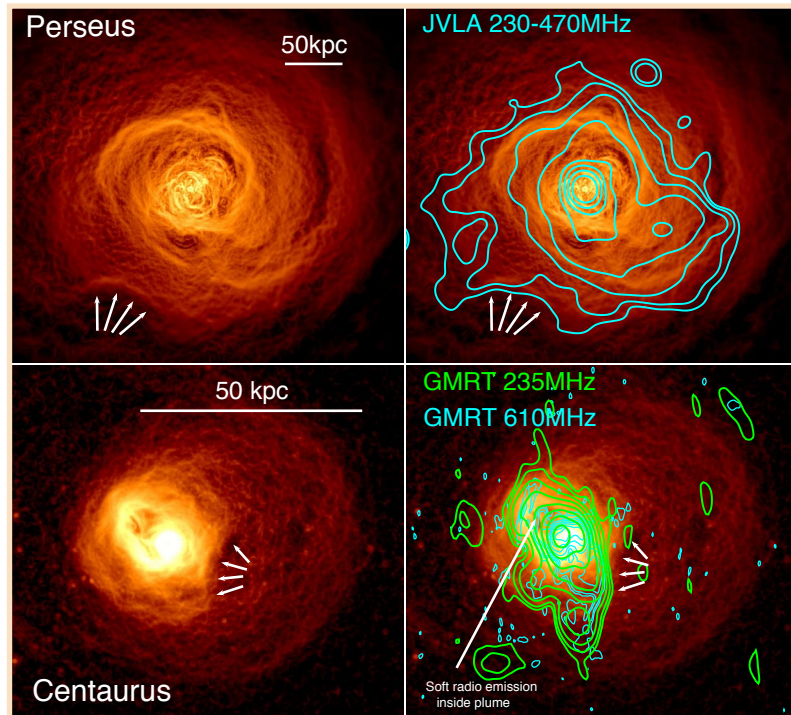


Figure 3. The left column shows multi-scale GGM filtered images of the Perseus cluster (top) and the Centaurus cluster (bottom). In the right hand column, radio contours are overlaid which appear to be constrained behind the concave ‘bay’ features. Adapted from Walker et al. (2017).

Assessing the significance of features

Although gradient filtering is a great tool to find structures, care must be taken to ensure features are robust. As we see in Figure 1, the noise in filtered images has a peculiar linear structure, unlike normal intensity images. Typically the filamentary features lie along surface brightness contours. For a fixed filtering scale, the noise increases towards regions with lower surface brightness. There are a number of methods to check for significance. These include examining the original unfiltered image in detail, for example by blinking between the original and the filtered image, making surface brightness profiles across a structure and looking at filtered model images fitted to the original image. Optimization of the position-dependent length scales used in gradient filtering to improve significance and reduce the noise is a current area of research.

We eliminated AGN feedback activity as an explanation because the bays are often one-sided, whereas AGN inflated cavities are often double-sided and correlated with jets launched by the central AGN.

Comparing to models of empty cavities in the intracluster medium, the observed surface brightness drop is too small, while the observed temperature jump is too large. If we try to increase the temperature jump in the cavity model by assuming a cavity which is highly elongated along the line of sight, the discrepancy between the surface brightness profiles becomes even larger. No geometry of cavity is able to reproduce the observations. Across the bay edge the temperature increases as the density decreases (on scales of the order of the Coulomb mean free path), similar to cold fronts, however, bays are concave, while cold fronts are convex.

When we compare observations to sloshing simulations (ZuHone et al. 2011, ZuHone et al. 2016) we find that, for the Perseus cluster, the bay position, size and morphology all bear striking similarity to the large (~ 50 kpc) KHI that form in these simulations (Figure 4). The magnitudes of the temperature and surface brightness jumps are also in good agreement between the simulations and the observations.

The morphology of the central radio emission in the clusters provides further clues to the nature of the bays. Cavities inflated by AGN are typically filled with radio emission from the diffuse relativistic plasma they contain. Cold fronts on the other hand typically constrain radio halos behind them. When deep radio observations of the central regions of Perseus and Centaurus are overlaid on the X-ray images (Figure 3) we see that the radio contours are confined to regions behind the bays. In Perseus the radio halo has exactly the same concave curvature along the edge of the X-ray bay. This is exactly what would be expected if the bays are concave cold fronts that result from the large KHI such as those predicted by simulations (ZuHone et al. 2011).

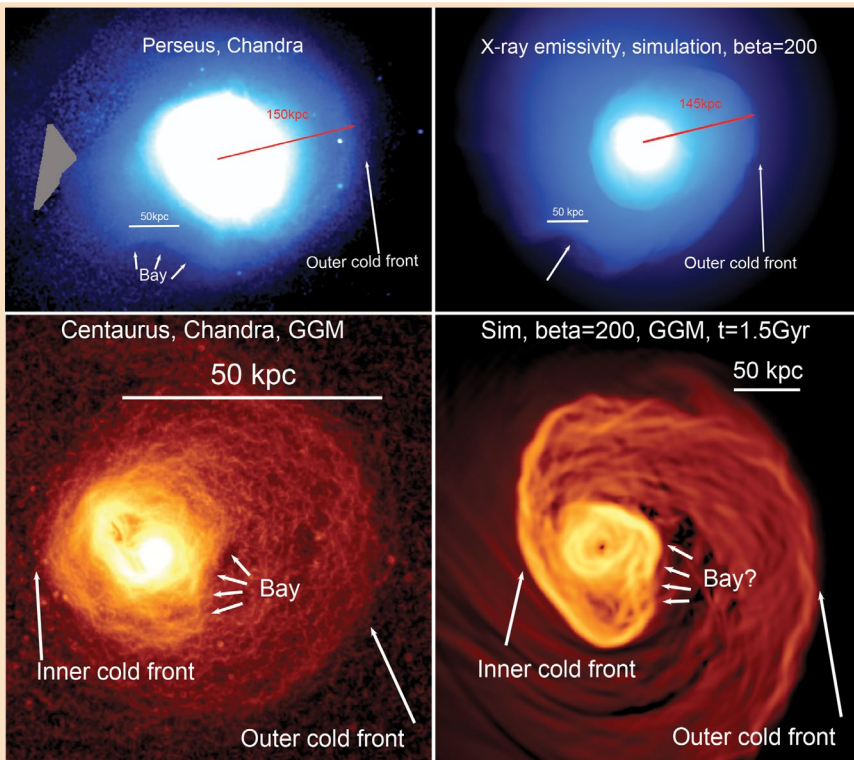


Figure 4: Comparing the locations of the bays in Perseus and Centaurus (left column) with the sloshing simulations from ZuHone et al. 2011 (right column). We are able to find good matches for the bay features in different time epochs of the simulations. Adapted from Walker et al. (2017). Grey triangular region in upper left panel is due to a gap in the coverage of the cluster.

More Subtle KHI Features in Centaurus and Abell 2142

When we apply the GGM filter technique to the *Chandra* images of the Centaurus cluster (Sanders et al. 2016a) and Abell 2142 (Walker et al. 2016), shown in Figure 5, we find linear features behind their main cold fronts, (features marked as L1, L2 and L3 for Centaurus, and marked by the white arrows for Abell 2142). These may be evidence for more subtle KHI (Roediger et al. 2011; ZuHone et al. 2011).

A Quick Way to Map the Width and Jump Ratios Along Cold Fronts.

As GGM images are maps of the gradient of the X-ray surface brightness, they provide a straightforward way to map variations of the jump ratio and width of cold fronts along their lengths. Typically such measurements require a lengthy process of dividing the cold front into multiple sectors and fitting each sector's surface brightness profile with a model consisting of a broken powerlaw smoothed by a Gaussian. Applying this technique to Abell 2319 and Abell 3667 (Figure 6, Walker

et al. 2016), we found that the gradient varies along the cold fronts. For A2319 the gradient is highest to the north (position A), and decreases to the south as we move to position B. For A3667, the gradient is highest in the middle of the cold front, and decreases on either side. By comparing to surface brightness profile fitting (Figure 6), we see that for A2319 this gradient decrease occurs because the width of the cold front increases along its length while its jump ratio is constant. By contrast, for A3667, the width is relatively uniform along its length, and the gradient peak in the middle is caused by the jump ratio being higher in the middle of the cold front.

Edge Detection in Simulations of the Intracluster Medium

Similar imaging analysis can be applied to simulations of galaxy clusters as well. This opens up the possibilities of using the comparison of the simulated images with the observations to explain the origin of certain edge features (such as the “bays” described above) or discriminating between different physical properties of the ICM. Such comparisons involve producing 2D projections of the X-ray emission expected from 3D hydrodynamic models of the cluster gas from simulations and filtering them

using the GGM technique.

Due to their origin in the relative motion of cold and hot gases in the ICM, cold fronts produced in simulations are associated with strong velocity shears, making them susceptible to the effects of KHI. KHI can be suppressed, to a degree, by viscosity or magnetic tension, implying that the properties of KHI in observed cold fronts can place constraints on these properties of the cluster plasma.

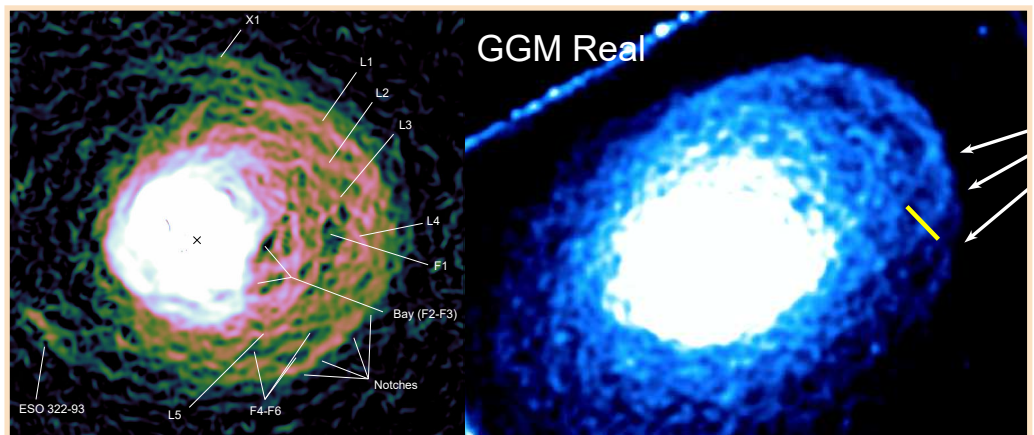


Figure 5. GGM filtered images of Centaurus (left from Sanders et al. 2016a) and Abell 2142 (right). We find linear features behind the cold front highlighted by the white arrows (features L1, L2 and L3 for Centaurus), which may be evidence of subtle KHI rolls. See Sanders et al. (2016a) for discussion of the notches indicated in the image of Centaurus (left). X-ray surface brightness profiles of ripples along the yellow line (in right panel) are studied further in Walker et al. (2016).

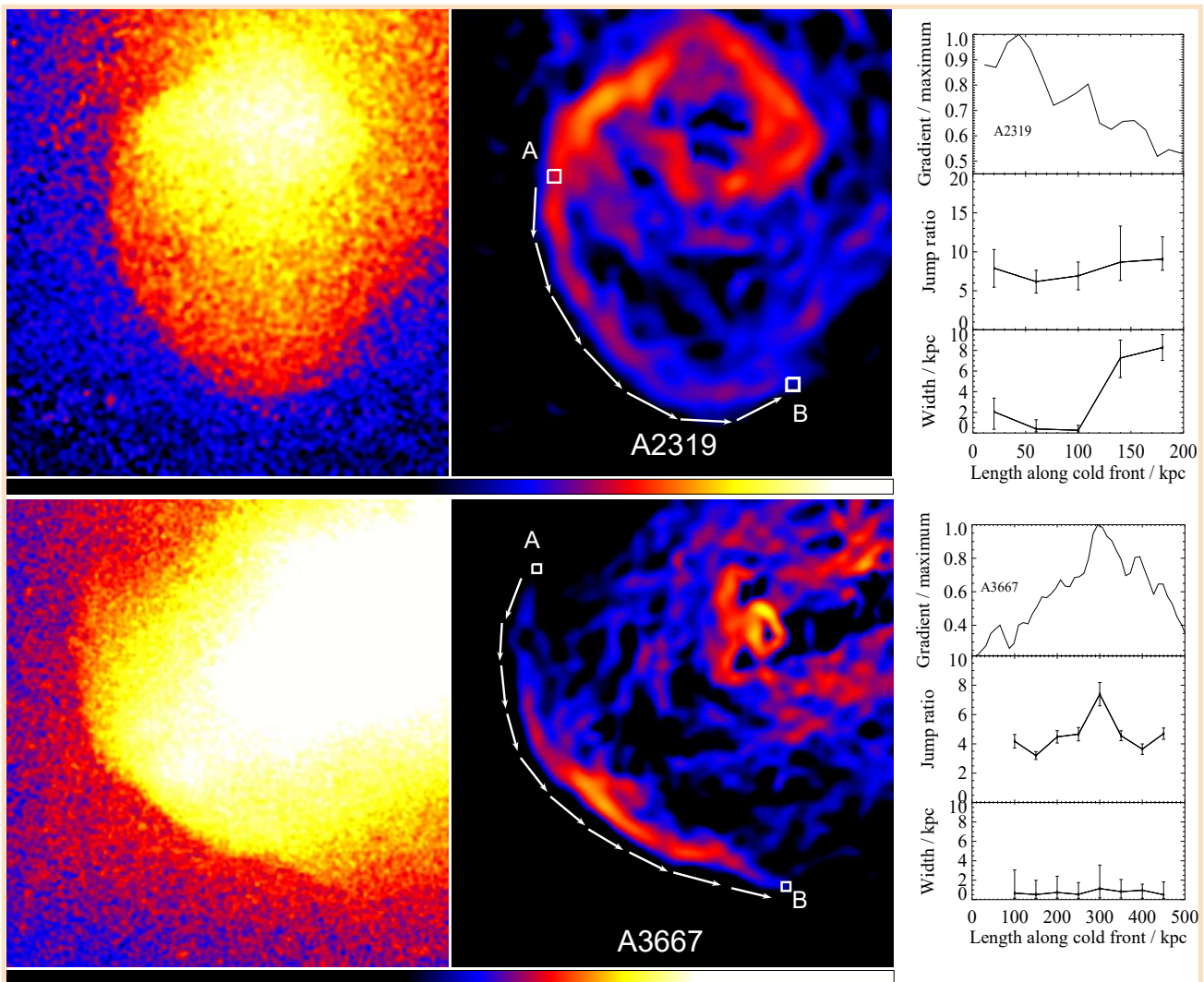


Figure 6. Looking at gradient variations along the lengths of the cold fronts in A2319 (top row) and A3667 (bottom row). On the left is the initial *Chandra* image, in the middle is the GGM filtered image, and on the right are the variations of the GGM magnitude, the jump ratio and the cold front width along the lengths of the fronts from position A to position B. Adapted from Walker et al. (2016).

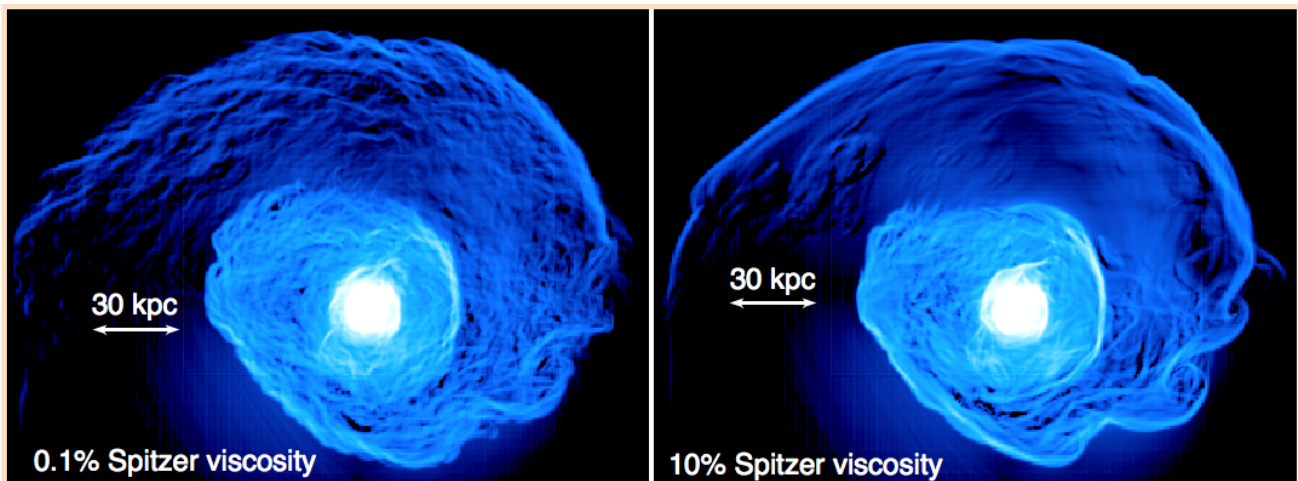


Figure 7: Sobel-filtered images of X-ray surface brightness from simulations of the Virgo cluster with varying viscosity. Viscosity smooths out the large cold front edges and reduces the number of smaller edge features produced by turbulent gas motions under the fronts. Reproduced from Roediger et al. (2013).

ZuHone et al. (2015) presented simulations of the Virgo cluster with varying viscosities and magnetic field strengths, and determined that a variety of the models for viscosity and moderately strong magnetic fields could result in cold fronts with similar appearance. This points to the main difficulty with using analysis of KHI at cold front surfaces alone to distinguish between the effects of these two distinct properties of the ICM, and suggests that other properties of the cluster gas should be examined to potentially break this degeneracy.

As previously noted, Roediger et al. (2013) used a Sobel filter to analyze images of X-ray surface brightness produced from simulations of the Virgo cluster (Figure 7). They examined hydrodynamic simulations with varying strengths of viscosity, and noted two distinguishing features in the filtered images. In the more viscous simulation, the cold front is a sharp continuous arc, whereas in the less viscous simulation it is distorted. Secondly, the filtered image revealed a wealth of structure in the low-viscosity simulation, produced by the undamped turbulent flow underneath the front surfaces.

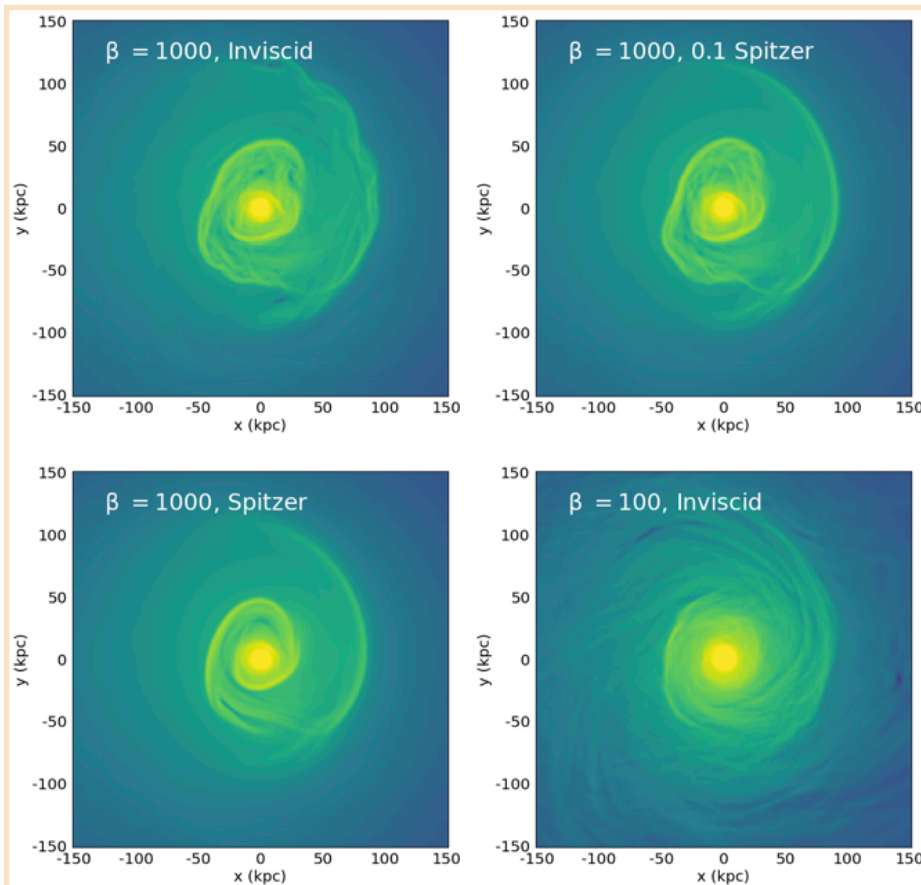


Figure 8: GGM-filtered images of X-ray surface brightness from four simulations from ZuHone et al. (2015), with varying magnetic field strength parameterized by the plasma β parameter and variations in viscosity given as a fraction of the *Spitzer* value given the local plasma properties. Increasing viscosity smooths out cold fronts and small-scale fluctuations, whereas increasing the magnetic field smooths out cold fronts but stretches fluctuations perpendicular to cold fronts, producing a banded structure underneath the front (Bellomi et al. 2018, in preparation).

Bellomi et al. (2018, in preparation) performs a similar analysis using the GGM filter on simulated X-ray images of cold fronts in a galaxy cluster core from the MHD simulations from ZuHone et al. (2015), who simulated a parameter space over magnetic field strength and viscosity. They confirm that increasing the viscosity smooths out the cold fronts and reduces smaller-scale edge features produced by the turbulence, which is damped out by higher viscosity (top-left, top-right, and bottom-left panels of Figure 8). In the case of an increased magnetic field (parameterized by the plasma β parameter, which is the ratio of the thermal to the magnetic pressures), though the cold fronts are indeed smoothed out, the edge structures underneath the front remain, but with a distinctly different character. The stretched and amplified magnetic field under the front produces long, band-like edge structures which vary in surface brightness primarily along the radial direction, correlating with small variations in the magnetic field strength. These very different signatures in surface brightness provide a potential opportunity to distinguish between the two ICM

properties of viscosity and magnetic field strength.

The primary challenge in discerning plasma properties such as these from edge-filtered images from real observations is that of statistics. As noted above, not all structures seen in the images are physical—the small-scale “wormy” features in particular are artifacts of the Poisson noise inherent in the X-ray images. Thus, definitively distinguishing between the different physical processes operating in the ICM as demonstrated above in the noiseless simulated images would require a very high signal-to-noise ratio in addition to high spatial resolution. Given the decrease of the low-energy response of *Chandra*/ACIS, such an analysis is likely out of its grasp (with the possible exception of the Perseus cluster), but would be well within the capabilities of *Lynx* (see Figure 9). Future work using realistic mock X-ray observations of simulated clusters will determine what observational capabilities would be required to use this technique to further elucidate the plasma physics of the ICM. ■

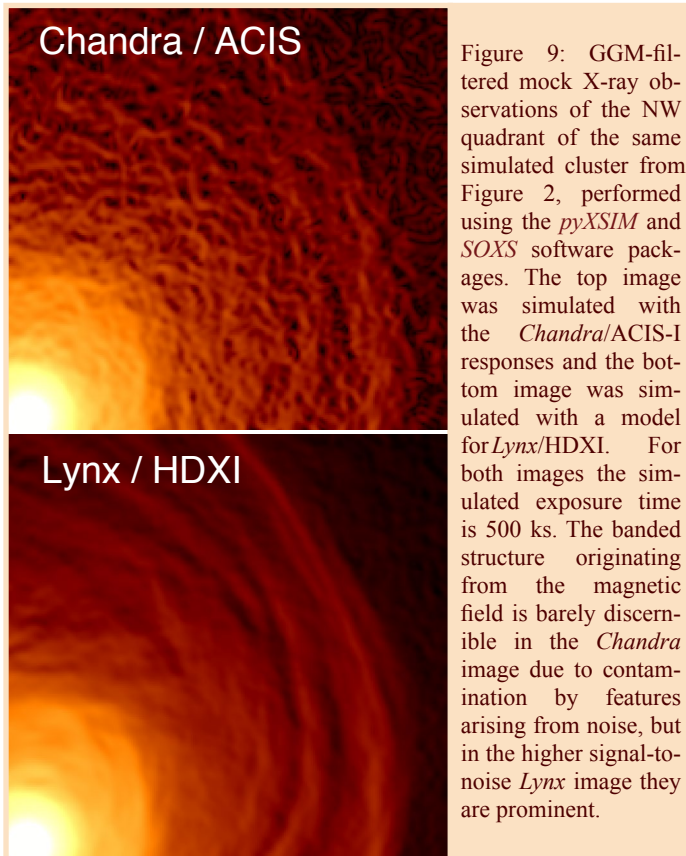


Figure 9: GGM-filtered mock X-ray observations of the NW quadrant of the same simulated cluster from Figure 2, performed using the *pyXSIM* and *SOXS* software packages. The top image was simulated with the *Chandra*/ACIS-I responses and the bottom image was simulated with a model for *Lynx*/HDXI. For both images the simulated exposure time is 500 ks. The banded structure originating from the magnetic field is barely discernible in the *Chandra* image due to contamination by features arising from noise, but in the higher signal-to-noise *Lynx* image they are prominent.

REFERENCES

- Fabian A.C., Sanders J.S., Allen S.W., Crawford C.S., Iwasawa K., Johnstone R.M., Schmidt R.W., Taylor G.B., MNRAS, 2003, 344, L43
 Forman W., et al., 2007, ApJ, 665, 1057
 Grebenev S.A., Forman W., Jones C., Murray S., 1995, 445, 607
 Laing R.A., Bridle A.H., 2013, MNRAS, 432, 1114
 Malin D.F., Zealey W.J., 1979, Sky and Telescope, 57, 354
 Markevitch M., Vikhlinin A., 2007, Physics Reports, 443, 1
 Marshall H. L., Miller B. P., Davis D. S., Perlman E. S., Wise M., Canizares C. R., Harris D. E., 2002, ApJ, 564, 683
 Roediger E., Bruggen M., Simionescu A., Bohringer H., Churazov E., Forman W. R., 2011, MNRAS, 413, 2057
 Roediger E., Kraft R. P., Forman W. R., Nulsen P. E. J., Churazov E., 2013, ApJ, 764, 60
 Sanders J.S., Fabian A.C., 2002, MNRAS, 331, 273
 Sanders J.S., Fabian A.C., 2008, MNRAS, 390, L93
 Sanders J.S., Fabian A.C., Taylor G.B., Russell H.R., Blundell K.M., Canning, R.E.A., Hlavacek-Larrondo J., Walker S.A., Grimes C.K., MNRAS, 2016a, 457, 82
 Sanders J.S., Fabian A.C., Russell H.R., Walker S.A., Blundell K.M., MNRAS, 2016b, 460, 1898
 Sanders J.S., Fabian A.C., Russell H.R., Walker S.A., 2018, MNRAS, 474, 1065
 Walker S. A., Sanders J. S., Fabian A. C., 2016, MNRAS, 461, 684
 Walker, S. A., Hlavacek-Larrondo, J., Gendron-Marsolais, M., et al., 2017, MNRAS, 468, 2506
 Young A. J., Wilson A. S., Mundell C. G., 2002, ApJ, 579, 560
 ZuHone J. A., Markevitch M., Lee D., 2011, ApJ, 743, 16
 ZuHone, J. A., Kunz, M. W., Markevitch, M., Stone, J. M., & Biffi, V. 2015, ApJ, 798, 90
 ZuHone J. A., Kowalik K., Ohman E., Lau E., Nagai, D. 2018, ApJS 234, 4

Director's Log, *Chandra* Date: 634348806

Belinda Wilkes
@BelindaWilkes

Over the past year, in addition to continued, highly successful operations and science, *Chandra* has been involved in a number of unusual, unexpected, and/or exciting activities. It has been a year in which the extended team has again, frequently and reliably, demonstrated the talent and dedication which make *Chandra* such an interesting, exciting and amazing mission with which to be involved.

The month of August was the most memorable. As we geared up for the Solar Eclipse on 21st August, for which many of us were traveling to the HEAD meeting (strategically placed and timed well in advance) in Sun Valley Idaho, LIGO reported its first trigger on a NS-NS merger, GW170817, quickly followed by a Fermi gamma-ray detection of a faint, short GRB. The LIGO-linked astronomical community went wild, scrambling to observe the source in as many wavebands and with as many facilities as possible in order to detect, track and characterize the first GW-source electromagnetic (EM) counterpart. *Chandra* was no exception. Three teams triggered pre-approved ToO observations, eventually resulting in three observations, the first two days after the LIGO trigger, and two more observations over the next two weeks. In order to be certain a strong detection was made before the source went behind the sun, we also approved a DDT observation, providing proprietary access to all three teams. Still embargoed (by the LIGO collaboration) ATELS abounded, papers were prepared, rumors flew, journalists became adept at pouring through mission observation logs and contacting astronomers in an attempt to learn what was going on. The “best known secret” in astronomy came to a head on 16th October at a dual press conference reporting all aspects of the discovery to date. The initial non-detection and subsequent detections in the X-rays were pivotal in confirming the source to be an off-axis short GRB (http://chandra.harvard.edu/press/18_releases/press_011818.html, and Project Scientist's report on page 10).

Chandra observations of GW170817 continued, using DDT time with publicly distributed data. Observations in early December, as the source transitioned from sunblock, showed that it had brightened in concert with the radio flux, confirming synchrotron as the emission mechanism in both wavebands. Possible explanations for the source of the emission include: a cocoon of gaseous debris heated by a failed off-axis jet; a structured relativistic jet in which our line-of-sight passes through wider, less-relativistic wings on the outer edge; or a quasi-spherical, mildly-relativistic outflow of debris (Mooley et al. 2018, Ruan et al. 2018,

Margutti et al. 2017). The January *Chandra* observations are now complete and may help to constrain these various possibilities. This first EM detection of a LIGO GW source heralds a new era in astrophysics, deemed “multi-messenger”, in which GW detectors will work in concert with multi-wavelength (radio-gamma-ray) EM astronomy to observe and study the densest objects in the Universe.

“What about the Solar Eclipse?”, you may ask. Well...I witnessed it happen, exactly as and when predicted, on Aug 21st 2017, along with a large fraction of the citizens and residents of our nation, and people from around the world. It was my first time, and an unexpectedly profound and moving experience astronomically, personally and socially, bringing tears to my eyes and a shiver down my spine. So many people worldwide united to watch the amazing and once-scary phenomenon of the sun disappearing, for all too short a time, in the middle of a cloudless, (for me) warm day in the hills of Idaho. I am hooked and already looking for the next one!

Our summer workshop: “From *Chandra* to *Lynx*: Taking the Sharpest X-ray Vision Fainter and Farther”, brought together >100 scientists to leverage *Chandra*’s legacy and maximize its impact on the development of the *Lynx* mission concept. *Lynx* promises to be a true *Chandra* Successor, aiming to continue *Chandra*’s unique, high-resolution quest, and to look much deeper into the otherwise invisible X-ray Universe. The workshop was a great success (see article on page 23 for a review). One major result of these discussions was the release of a Special Call for *Chandra* proposals for pathfinder science to demonstrate the feasibility of a *Chandra* Successor Mission (CSM) and for which up to 1 Ms of DDT time are being made available. The initial call for White Papers, to assess the level of interest and feasibility, resulted in 29 responses—more than expected—and a review panel of external and internal scientists recommended that the Special Call go forward. Twenty-seven CSM proposals were received by the 24 Jan deadline. A review panel was convened on 14 Feb and recommended that 3 proposals be approved. The results were announced on 23 Feb and can be found at: http://cxc.harvard.edu/target_lists/cycle19/csm_cyc19.html. Approved observations will be scheduled as early as is possible given the combination of observational and feasibility constraints. The aim is to allow the results to be included in the case for a *Chandra* Successor Mission being submitted to the 2020 Decadal Survey.

The Cycle 19 proposal call included a number of updates which were the result of various community discussions including: the 2016 summer workshop (<http://cxc.harvard.edu/cdo/cxo2lynx2017/>), the *Chandra* Users’ Committee, direction from NASA in 2016 to ensure that we maximize the science of NASA’s missions, and attendance by various *CXC* staff at several multi-wavelength transient

science meetings over the past 2–3 years. First, we once again included Very Large Projects (>1 Ms of time), which resulted in the approval of 2 VLPs including ~2.6 Ms of observing time. Second, we negotiated an increased amount of joint observing time to be made available for *HST*, *XMM-Newton*, and *NuStar* joint programs, reserving these new allocations for LP and VLP *Chandra* proposals. Third we were able to increase by 50% the amount of funding allocated to archival programs in Cycle 19, which resulted in the approval of a record number of 24 archive proposals. In addition, following discussion at the Jan 2017 meeting of NASA mission leaders convened at NASA’s request by *CXC* (Wilkes) and *HST* (Wiseman) at the AAS, we have continued to consult with other observatories, in particular *NuStar*, to plan a one-stop website which will provide easy access to the planned and as-run observing schedules of as many observatories as possible. This will not only increase communication on observation planning, particularly important for the transient science community, but will also facilitate maximization of science by coordinating multi-facility observations when possible, even when this is not part of an approved joint program.

Over the past year, *Chandra* has continued its excellent performance, observing at high efficiency despite the continued challenge of maintaining the thermal balance of the various subsystems as the thermal insulation degrades. In Cycle 20 there continues to be only one limitation on proposal submission as a result of the operational complexities: a maximum of 2 Msec of observing time will be allocated within 60 degs of the ecliptic poles to Large and Very Large programs (Sect 4.2 of the *CfP*). With the release of the Cycle 20 Call for Proposals, we also released an update of our science website (<http://cxc.harvard.edu/>), and seek your comments on this redesign. Science highlights for the year, in addition to the GW 170817 observations, included observations of Jupiter in concert with the Juno satellite which detected X-ray aurorae at both north and south poles (<http://chandra.harvard.edu/photo/2017/jupiter/>, also see the HRC article on page 13), observations of Sgr A* and M87 coordinated with the first major EHT observing run in April (results still TBD), and the multi-wavelength (X-ray, radio, optical) picture of merging cluster Abell 3411-3412 on the cover of the first issue of *Nature Astronomy* (http://chandra.harvard.edu/press/17_releases/press_010517.html).

Another major activity for 2017 was the submission of a proposal to extend the *CXC* contract to continue *Chandra* operations from 2018–2027, including a three-year close-out period to 2030. This is aimed at replacing the current *CXC* contract between NASA and SAO to operate *Chandra* through Sept 2018 followed by a one year close-out. A new, major, unexpected activity, which will take around two years to complete, is the move of the Opera-

tions Control Center from its current location in Kendall Square, Cambridge to a location in Burlington, off Rt 128. This necessity is due to our present landlord being unable to extend our lease past Sept 2019. Planning for the move is already well along, thanks to the huge efforts of many CXC, NASA and Smithsonian staff, under the leadership of CXC Manager, Roger Brissenden (see the Program Manager's Report on page 11 for more details). NASA has transitioned its Senior Review of operating missions to a three-year cycle, so the next will take place in early 2019 rather than this coming year, a welcome relief given the activities described above. On a somber note, we suddenly and tragically lost our long-time, charismatic, Lead Mission Planning Engineer, Brent Williams, in early November (see article on page 20). The incredible turnout (>1000 people) at his funeral events was a visual and humbling testament to the number of lives he touched, well beyond those at the CXC who miss him every day.

The Einstein Fellows Program, formerly managed by the CXC, has completed its transition, along with *Hubble* and Sagan Fellows, to a merged NASA *Hubble* Fellowship Program (<https://nhfp.stsci.edu/>). This merged program is being hosted by STScI and administered jointly by the three leads from CXC, NeXSci and HST. Applications were submitted via a single portal and were assessed by joint review panels who met in Washington DC in late January (see article on page 28).



Figure 1: Dr. Zurbuchen holding a supernova remnant in his hand at the *Chandra* booth at the AAS meeting



Figure 2: NASA hyperwall presentation on GW170817 by Dr. Melanie Nynka, McGill University.

The 2018 AAS in Washington, DC brought with it another opportunity to meet Dr. Thomas Zurbuchen, the NASA Associate Administrator for the Science Mission Directorate. Dr. Zurbuchen once again toured all the NASA mission exhibits, including the *Chandra* booth (Figure 1), spending significant time meeting and talking with staff. Once again several *Chandra*-related presentations were given at the NASA hyperwall, which provides a wonderful display to highlight the spectacular *Chandra* and multi-wavelength data (Figure 2). *Chandra* exhibit activities included: information and demonstrations of the *Chandra* Source Catalog V2.0, expected to be completed in early spring (see article on page 22); two VR activities: a 3D tour of the supernova remnant Cas A, and a simulated, dynamic, 4π view from Sgr A* of the surrounding stars, hot gas, and outbursting sources (the subject of a press release: <http://chandra.harvard.edu/photo/2018/gcenter360/>); communication products developed as part of the Universe of Learning NASA-CAN project, of which the CXC is a member; and a new educational activity. The booth was uniformly busy and great fun!

Finally, we are turning our eyes to the 20th anniversary, in 2019, of *Chandra*'s launch on the shuttle Columbia on 23rd July 1999. This is an amazing feat for a free-flying mission, and we have convened teams and committees to design, prepare, and produce products and events throughout 2019 in recognition and celebration. While planning is in the early stages, we expect to include a major science symposium, a reception in the Boston area, publication of an e-book on 20 years of *Chandra* science, and the release of anniversary products, articles, and presentations distributed throughout the year. Please stay tuned! ■

References

- Margutti et al. 2017, ApJL, 848, L20
- Mooley et al. 2018, Nature, 554, 207
- Ruan et al. 2018, ApJL, 853, L4

Project Scientist's Report

Martin C. Weisskopf

Now in its 19th year of operation, the *Chandra* X-ray Observatory continues to provide unique capabilities for high-resolution X-ray imaging and spectroscopy, enabling high-impact research by the astrophysics community. This was outstandingly confirmed through the use of Director's Discretionary Time (DDT) this past year to search for, and ultimately observe, X-ray emission to a high degree of localization from the aftermath of the collision of two neutron stars. The use of DDT facilitated making the results of the *Chandra* observations to the broad community. The image below shows the continued brightening of the X-ray counterpart (courtesy of the CXC and John J. Ruan et al., *Astrophysical Journal Letters*, Jan. 18, 2018).

The *Chandra* Team continue maximizing the scientific performance and observing efficiency of the Observatory, especially important as NASA and other international space agencies develop their plans for the next-generation facility-class X-ray missions such as *Lynx*.

As noted in the Project Scientist's Reports in previous issues of this Newsletter, three problems are gracefully degrading the Observatory's performance as it ages: (1) thermal warming, (2) radiation damage, and (3) molecular contamination. Here we provide a brief update on the status of each of these issues.

1: Increased heating of some spacecraft subsystems at particular Sun attitudes, due to degradation of the multilayer insulation blanketing the Observatory, introduces complexity in the routine operation of *Chandra*. Significant thermal modeling efforts have been undertaken to provide robust predictions for the time behavior of on-board temperatures for particular spacecraft attitudes relative to the Sun, and these models have been successfully integrated into tools used to generate both long-term and short-term schedules of observations. In addition, these models have been incorporated to introduce small pointing offsets based on predicted thermal profiles in order to ensure that the accuracy for target placement on the focal plane detectors remains within the original

Observatory specifications. These efforts have resulted in an ability to maintain *Chandra*'s excellent performance and high observing efficiency, (nearly 70%). While this situation does not yet present thermo-mechanical problems, there is potentially an issue concerning molecular contamination (item 3 below), as components out-gas and off-gas more rapidly at higher temperatures.

2: After radiation damage to the ACIS front-illuminated CCDs during unprotected radiation-belt passes early in the mission, the CCDs continue to exhibit acceptably slow rates of Charge Transfer Inefficiency (CTI) increase. Although the Sun is approaching solar minimum in 2020 or so, there were two intense periods of activity during 2017, the second period (in September) resulting in interruption of science operations to shield ACIS. As low-energy (0.1–0.5 MeV) protons in the radiation belt caused the initial damage to the CCDs, the *Chandra* team monitors low-energy protons using NOAA-provided real-time solar-wind data from the Advanced Composition Explorer (ACE). Although ACE is no longer the primary real-time space-weather satellite at L1, NOAA has been able to provide about 70% ACE coverage, which is adequate for the *Chandra* purposes

3: The *Chandra* calibration team continues to monitor accumulation of molecular contamination on the ACIS optically blocking filters (OBFs). The team regularly releases updates to the calibration files that account for increasing x-ray attenuation, especially at low energies, by the contamination layer. Calibration observations are conducted several times during the year to characterize the temporal evolution of the contamination layer. When the current performance deviates significantly from the existing calibration file, an updated file is created and released for use by the GO community. There are no plans to bake-out the ACIS filters in the near term; however, risk/benefit considerations continue to be reviewed. ■



Figure 1: The image shows the continued brightening of the X-ray counterpart (courtesy of the CXC and John J. Ruan et al., *Astrophysical Journal Letters*, Jan. 18, 2018).

Project Manager's Report

Roger Brissenden

Reporting Period: January–December 2017

Chandra has carried out more than 18 years of highly successful and productive science operations. The *Chandra* X-ray Observatory is unique in its capability for producing the sub-arcsecond X-ray images that are essential to accomplish the science goals of many key X-ray and multi-wavelength investigations in current astrophysical research. The Project is looking forward to many more years of scientific productivity. NASA has chosen to continue the mission, and SAO and Marshall Space Flight Center are working to extend the contract to operate the *Chandra* X-ray Center with options through September 2030.

In conjunction with the *CXC* contract extension, the *Chandra* Operations Control Center (OCC) will move to a new location. Since the start of the mission, the control center has been located at a Draper Laboratory building in Cambridge, MA. Because the Draper lease will not be extended, a new location has been selected in Burlington, MA. The lease for the new property has been signed, and following buildout over the summer, the team will outfit and test the new facility with the necessary operations equipment, with a plan of transferring operations to the new OCC in the spring or early summer of 2019.

The Observatory continues to operate extremely well overall but with a number of incremental changes in performance, due primarily to the gradual accumulation of molecular contamination on the UV/Optical blocking filter that protects the ACIS detector, and to progressive degradation of the spacecraft's thermal control surfaces. Condensation on the UV/Optical blocking filter reduces ACIS's sensitivity to low-energy X-rays (but does not affect the HRC). The *CXC* calibration group continues to monitor the contamination layer and to update calibration files as needed so that Observers can analyze their data properly.

The decline in insulation effectiveness requires extra effort in scheduling observations and the use of special strategies to ensure continued safe operation in the evolving thermal environment, but has not significantly affected *Chandra*'s observing efficiency.

The combined effects of accumulated radiation damage and increasing temperature on *Chandra*'s aspect camera CCD have begun to affect the camera's ability to detect faint stars. Left unchecked, this trend would present difficulty in acquiring and tracking guide stars, which could decrease mission efficiency or preclude observation of some targets. Several mitigation strategies have been successfully implemented, including development of an update to the aspect camera processor software that improves the robustness of star tracking.

The Operations team responded extremely well to anomalies on four occasions since December 2016, when the spacecraft failed to acquire the expected aspect guide stars following a maneuver. In these cases, *Chandra*'s science program was stopped but the spacecraft redundancy configuration remained unchanged, allowing for rapid diagnosis and return to science. Two independent root causes for the anomalies have been determined, the first relating to the effect of increased noise in the gyro bias rate during a maneuver, and the second, to the aspect camera tracking hot pixels during the prior observation. Neither of the causes relates to a new concern about the hardware, but rather, are typical of the engineering trends being managed by the operations team as the spacecraft ages. A number of near-term mitigations have been implemented in order to minimize recurrences and the team is working on strategies to address the issues over the longer term.

During September the Observatory interrupted science observing on two occasions due to increased solar radiation, resulting in a total of 290 ks of science time lost but no harm to *Chandra*'s instruments. One of the interruptions occurred shortly after *Chandra* emerged from the Earth's radiation belts, revealing the need for a revised radiation safing protocol to protect the High Resolution Camera in such an unusual situation. Appropriate processes have now been put in place.

The *Chandra* Source Catalog team published on-line an updated preliminary detection list for *Chandra* Source Catalog 2.0 (list *CSC 2.0 pd2*, see <http://cxc.cfa.harvard.edu/csc2/>). The list provides an initial set of key data, including positions, likelihoods, amplitudes and associated errors, for all of the ~374,000 detections that will be included in the full catalog to be released in early 2018. A pre-release source list including ~316,000 unique X-ray sources on the sky was published in November. In December, the team began preparing source properties, such as fluxes and spectral measurements, of fully processed sources for public dissemination. As of the end of the year, properties for ~110,000 sources were available, about a third of the expected total.

In response to the December 2016 call for proposals for Cycle 19 observations, scientists worldwide submitted 574 proposals, including 462 proposals for observing and 112 for archive and theory research. The Cycle 19 peer review, held in June 2017, approved 122 observing proposals, including 7 Large Projects and 2 Very Large Projects, and 33 theory and archive investigations.

The call for proposals for Einstein fellowships attracted 163 applications for 2017. The 8 Fellows selected in January by the Einstein Fellows peer review began their three-year terms in Fall of 2017. Because NASA is in the process of consolidating its named fellowships programs under the administration of the Space Telescope Science Institute, this is the final group of *CXC*-administered Einstein Fellows.

The CXC held a workshop, “From *Chandra* to *Lynx*: Taking the Sharpest X-ray Vision Fainter and Farther”, in August 2017. *Lynx*, formerly known as the X-ray Surveyor, is one of the large strategic mission concepts being studied by NASA in preparation for the 2020 U.S. Decadal Survey. *Lynx* is the first future X-ray mission concept planned to match the spatial resolution of the *Chandra* X-ray Observatory. This workshop sought to leverage *Chandra*’s legacy and maximize its impact on the development of *Lynx* science and design objectives. Information about the workshop is available at <http://cxc.harvard.edu/cdo/cxo2lynx2017/>.

The *Chandra* Press Office has been active in issuing image releases, science press releases and other communications of *Chandra* research results. A complete listing is available at <http://chandra.harvard.edu/press/>.

The annual Newsletter (#24), which was released and distributed in April, can be found online at: <http://cxc.harvard.edu/newsletters/>. Information about the *Chandra* Observatory and the *Chandra* X-ray Center can be found at <http://cxc.harvard.edu/>. ■

ACIS Update

Catherine Grant, for the ACIS Team

The ACIS instrument continues to perform well and produce spectacular scientific results like the recent X-ray detection of the LIGO-discovered neutron star merger. This is reflected in the proposal statistics for Cycle 19 in which ACIS was five-times oversubscribed. There were no interruptions of scheduled observations due to ACIS anomalies in the past year and there are no instrument limitations on continued operation of ACIS indefinitely into the future. The calibration team continues to monitor the loss in QE due to the contamination layer and the charge transfer inefficiency due to radiation damage.

As the observatory ages, thermal blankets covering the surface continue to degrade, which tends to make many systems run hotter. This can be managed by careful mission planning, and in the case of ACIS, dropping optional CCDs. In Cycle 20, the RPS form will allow proposers to the Guest Observer programs (GOs) to specify a maximum of four required CCDs at the time of proposal submission due to thermal considerations. In addition to the four required CCDs, a GO may request that one or two optional CCDs be turned on for an observation if thermal conditions allow. If the science requires that five or six CCDs be on for an observation, the GO may work with their User Support scientist to change the CCD specification but they should be aware that this might complicate the scheduling of their observation. (See section 6.22.1 in the POG for details.)

The mission planning depends on detailed semi-empirical thermal models of the focal plane, electronics boxes and boards, and power supplies. Much work has gone into updating these models to keep the predictions accurate, so

that we can confidently operate without violating thermal limits. In early 2018, the ACIS operations team will modify the standard configuration during radiation belt passages to keep only three front-end processors (FEPs) powered instead of six. Previously, six FEPs had been powered on for radiation belt passages to keep the electronics relatively warm and to minimize temperature excursions, but given the elevated spacecraft temperatures, the ACIS electronics will be sufficiently warm with only three FEPs powered on.

While the sun has generally been very quiet—as is expected during solar minimum—there were two periods of much higher activity (mid-July and early-September of 2017) that impacted *Chandra*. Each of these were quite different, both in the energy spectrum of the particles and in the response by *Chandra*. After a few years of quiet time, this was a good opportunity for the operations team to exercise the high radiation response procedures.

In July, after an M-class solar flare, very high soft proton rates were reported by ACE (Advanced Composition Explorer), which is situated at the Sun-Earth L1 point. On-board *Chandra*, the radiation monitoring done by HRC and ACIS is most sensitive to harder particles, so while the detectors did see some elevation in particle flux, it was not high enough to trigger an autonomous radiation safing action. On the ground, the *Chandra* team examined the available data and decided not to interrupt the observing schedule. While the calculated attenuated fluence at ACIS was well over the orbital limit from this storm, the annual cumulative fluence is still far below the limit given the lack of radiation storms. No adverse effects have been detected from this event.

On September 6, 2017, the sun produced the largest X-class flare in a decade, which was followed a few days later by a nearly as powerful second flare. In both these cases, the particle spectrum was very hard, and two radiation shutdowns were triggered autonomously due to high rates in the HRC anti-coincidence shield. The ACIS radiation monitor also recorded very high rates, but did not trigger a shutdown due to the timing of the rise against the observation plan. The high radiation environment was long-lived causing *Chandra* to stay shut down for a few days. Again, no adverse effects to ACIS have been detected. The strong solar storm did, however, reduce the quiescent particle background rates measured by ACIS by about 10%, in what is known as a Forbush decrease. They have since recovered to the previous levels, typical of solar minimum.

Thinking ahead into the long-term future, the ACIS team has been developing and updating a set of operations procedures to deal with potential instrument anomalies and improved cataloging of the documentation of previous anomalies in case they reoccur. In this way, the historical knowledge of the software and hardware can be captured, which is increasingly important as key personnel move on to other projects or retire.

Another project intended to facilitate long-term operation of ACIS is monitoring the EEPROM (electrically erasable programmable read-only memory) devices in the ACIS Digital Processing Assembly. This non-volatile memory was last written twenty years ago, before launch, and contains, amongst other data, the boot code for the ACIS digital processors. The long lifetime of *Chandra* means there is little comparable data on the expected decay rate or operational lifetime of these specific devices. Starting in 2016, the ACIS team has done a monthly check of the active EEPROM, comparing the checksum of the actual contents to the expected value to identify potential bad memory locations. To date, these checksums have been identical, indicating that the contents of the active EEPROM are unchanged since before launch and free of bad memory locations. The portion of the EEPROM memory that is considered critical is actually fairly small, so any potential future bad memory locations will not necessarily require any changes in operations procedures. In the event that degradation impedes the normal function of the EEPROM, additional procedures to patch potential bad memory locations or to switch to the backup EEPROM are currently under development. ■

HRC Update

Grant Tremblay, Ralph Kraft, Paul Nulsen, Esra Bulbul, Dan Patnaude, & William Dunn

The High Resolution Camera (HRC) remains healthy and busy as ever, enabling legacy-class *Chandra* science with many high-impact results over the past year. One of these highlights is found in the shining poles of Jupiter, focus of a recent HRC observation designed to capitalize on a time when the planet's tilt relative to Earth provided excellent simultaneous views of both its northern and southern X-ray-bright aurorae. HRC's large field of view encompassed the entire planet as it rotated, and its exquisite spatial and temporal resolution revealed not only the morphology of X-ray emission at both poles, but also how the aurorae pulsed and shimmered in time.

In a paper recently published in *Nature Astronomy*, Dunn et al. compare the pulsations of the northern and southern auroral X-ray hot-spots. The team found that the periodicity and brightness of the northern and southern Jovian aurorae were largely uncorrelated, such that they pulsed almost completely independently from one another. This surprising result is highly unlike Earth, whose northern and southern aurorae mirror one another almost exactly. The implication, then, is that an asymmetric magnetospheric process may be at play on the Jovian day side, in tension with current models for the generation of these X-ray aurorae. *Chandra*/HRC and *XMM-Newton* will continue to monitor Jupiter's brilliant polar light shows over the next few years.

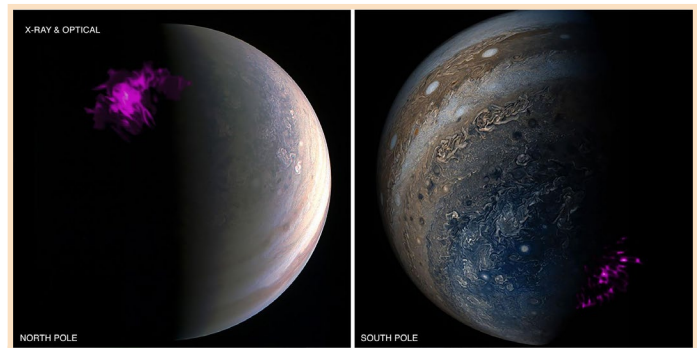


Figure 1: A *Chandra*/HRC and Juno composite of Jupiter and its stunning X-ray aurorae, shown here in purple. Credit: X-ray: NASA/CXC/UCL/W.Dunn et al., Optical: South Pole: NASA/JPL-Caltech/SwRI/MSSS/Gerald Eichstädt/Seán Doran; North Pole: NASA/JPL-Caltech/SwRI/MSSS. Science paper: Dunn, W.R. et al., 2017, *Nature Astronomy*, 1, 758.

In a powerful demonstration of the HRC's multiwavelength synergy, some of these observations will be coordinated with in-situ measurements during perijove passages of the Juno spacecraft, currently in polar orbit around the mighty planet.

While HRC instrument performance remains excellent and stable overall, it has long been known that the detector gain has been steadily declining since the beginning of the mission. This gain sag can slowly decrease quantum efficiency (QE) and increase spatial variations within the detector. As discussed in last year's newsletter, this issue is both understood and expected. Nevertheless, in an attempt to mitigate this sensitivity loss, the operating voltage of both HRC-S microchannel plates was increased in March of 2012, nearly restoring the instrument's sensitivity to what it had been at launch. The gain resumed dropping immediately following the voltage change, however, this time with a steeper decay rate. The gain sag has therefore "caught up", and is now roughly where it was just prior to the intervention in 2012. The instrument PI, Ralph Kraft, has commissioned an HRC Gain Working Group which, alongside the CXC Calibration group, is charged with better understanding and mitigating this loss of sensitivity for the HRC-S. In pursuit of the latter goal, the Calibration team may soon recommend that another voltage increase be implemented in the coming year.

Meanwhile, the HRC IPI and Calibration teams continue their work in optimizing the performance of the instrument. Recent progress has been made with regard to improving the background rejection algorithm, wherein background/non-X-ray events are vetoed based upon certain features of the electron cascade they create within the HRC's microchannel plates. While the *current algorithm* is excellent, it was developed at the beginning of the mission, so the team is now testing whether it can be made more effective with (slight) modifications. The HRC team will keep the community apprised of its progress as this project moves forward.

Finally, the HRC team is delighted to announce that it has grown with the recent hiring of Grant Tremblay and Esra Bulbul. Almus Kenter has recently taken up a Professorship in Maine, but remains part of the instrument team to support laboratory work and flight operations. ■

HETG Update

Hans Moritz Günther

HETG in Absorption

In this year's HETG update, I want to take the opportunity to delve deep into the relation between the HETG and absorption. There is some bad news (possibly with a work-around), but also some good news: On the one hand, the increasing contamination on ACIS reduces the effective area at the soft end of the HETG range so much that observations of e.g., stellar O VII triplets now require very long exposure times for all but the brightest stars. It seems that this trend will continue for the foreseeable future (L. David in this issue). In the first section of this article, I will show our efforts to open up a new mode for HETG users which would pair the HETG with the HRC to overcome this problem.

On the other hand, absorption in the far-away universe (as opposed to absorption on the CCD) is something that can help us learn about the structure of AGN and the properties of the intergalactic or interstellar medium. So, as a positive counterpoint, I'll highlight some recent use of the HETG to study absorption in the universe in a productive way.

Experimenting With a New Setup: HETG/HRC-I

The HETG is used almost exclusively with ACIS as a detector (there are only two exceptions to this rule in the entire history of *Chandra*, which I will discuss later), and if you use ACIS for grating spectroscopy, you want to use ACIS-S. As most readers of this newsletter surely know, ACIS-S consists of 6 CCDs arranged in a long array that catches both the positive and the negative diffraction orders of the HETG. The image on the detector has the form of an "X", because the HETG has two parts, the HEG (high-energy grating) and the MEG (medium energy grating), each of which is responsible for one of the legs of the "X" (Canizares et al., 2005). The CCDs of ACIS-S do not lie on a plane, instead they are tangential to the Rowland circle.

The Gunk and the Goo Steal our Soft Photons

The HETG disperses the photons, and the ACIS CCDs detect them. At least that's the plan. With increasing contamination on the ACIS chips, more and more of the soft photons are absorbed by the gunk and goo that sits on top of the ACIS filters. This is not so much an issue for the HEG, which is—surprise—most efficient for high-energy photons that pass through the absorbing layer, but more of an issue for the MEG.

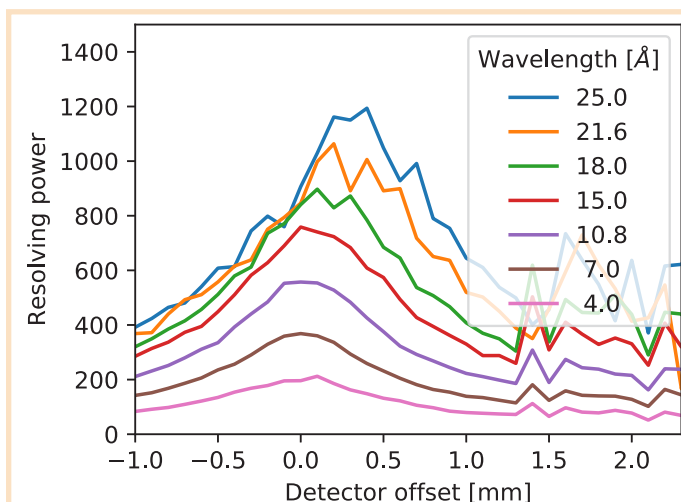


Figure 1: Expected spectral resolving power for HETG/HRC-I for different focus offsets based on MARX ray-trace simulations.

What Can We Do?

ACIS has been designed with the option of a bake-out, where the chips would be heated to remove all that gunk, but such a bake-out also poses a significant risk to the instrument (see, e.g., the Project Scientist's Report in the 2017 newsletter). Absent a bake-out, we have basically three options to mitigate the impact of the contaminant on HETG observations: (1) stop using the HETGS for any science case that requires data longward of 15 Å, (2) increase integration time for observations (in some cases, much much longer), or, (3) use a detector other than ACIS.

When *Chandra* was launched, there was a clear expectation what grating and detector combinations would be useful together and looking at all observations carried out in 2017, the community continues to follow that pattern. Excluding calibration observations, there were 88 observations with HETG and all of them use ACIS-S as the detector of choice; in the same year there were 26 LETG observations and all of them used HRC-S as detector. There is a good reason why this is the standard choice: ACIS is sensitive over the energy range covered by HETG spectroscopy and the intrinsic energy resolution of the CCDs allows the observer to separate the diffraction orders, thus making it much easier to analyze the extracted spectra compared to spectra acquired from the LETG/HRC-S combination where higher order photons are confused with the first order signal. However, the LETG more efficiently disperses longer wavelength photons where the ACIS sensitivity is low, thus making the HRC the detector of choice for LETG observations.

Could We Use HRC as a Detector for HETG Observations?

Let's just say that again: "the LETG more efficiently disperses longer wavelength photons where the ACIS sensitivity is low, thus making the HRC the detector of choice

for LETG observations”. With increasing contamination on the ACIS optical blocking filters, this statement starts to become true for HETG observations as well. To detect long wavelength photons with ACIS requires longer and longer integration times; thus, using the HETG with the HRC is an option worth investigating. However, there is no such thing as a free lunch. If we use the HRC, we can no longer rely on the CCD energy resolution to perform order sorting—just as it is true for LETG/HRC observations.

Motivation to Test HETG/HRC

If an observation aims specifically for diagnostics at relatively long wavelengths (say the O_{VIII} line at 18.97 Å, or the O_{VII} triplet around 22 Å), one might use the LETG instead of the HETG in the first place. However, we usually need to analyze all the signal that we can get. The HETG is ahead of the LETG in at least two areas: First, the HETG has a higher spectral resolving power than the LETG. If a science case requires the very best resolution we can get, then we have to use the HETG. Second, the HETG offers a higher effective area at wavelengths shortward of 15 Å. If the science requires good signal in this region, again, we have no choice but use the HETG.

As an example, consider the X-ray activity from classical T Tauri stars (Günther et al. 2010). These are young, low-mass, pre-main sequence stars in the phase of planet formation. They are still surrounded by an accretion disk, and mass falls from this disk onto the stellar surface where it forms an accretion shock. The shock is hot enough to be seen in X-rays. To measure densities and temperatures in the shock, the O_{VII} triplet (~22 Å) and the Ne_{IX} triplet (~13.5 Å) must be observed. The latter is often contaminated by Fe lines; HETG resolution is required to resolve those lines. Because the spectrum is dominated by known emission lines, order sorting is less of a problem than in continuum dominated sources—knowing the wavelength of the line enables the observer to distinguish between first and third order features.

One More Twist: HRC-I vs. HRC-S

Chandra has two HRC detectors, one optimized for imaging (HRC-I) and one for spectroscopic observations (HRC-S). Similar to ACIS-S, the HRC-S is made of segments that are mounted to approximate the Rowland circle. Most LETG observations use the HRC-S. However, the background in the HRC-S is much higher than in the HRC-I, because the anti-coincidence shield of the HRC-S is not functional. In fact, the background alone would saturate the *Chandra* telemetry, hence only limited regions of the detector can be sent to the ground. Since the LETG disperses the spectrum along a single line, the telemetry is not saturated. However, the two legs of the dispersed HETG spectrum spread across a larger chip region, in fact, so much larger that the most distant dispersed spectrum might fall off the chip. So, we opt to use the HRC-I as the detector. The HRC-I is not as long as the HRC-S, but HRC-I is large enough to capture essentially all the dispersed HETG spectrum. “But” I hear you say “HRC-I is flat!” and thus the spectrum will be out of focus. True, I say, but not very much. The distance between the flat HRC-I surface and the Rowland torus is small compared to the diameter of the Rowland circle (about 10 m) and the loss of resolving power is acceptable. Additionally, a user can adjust the focus position of the detector plane to determine exactly where the flat detector intersects with the Rowland circle. Figure 1 shows MARX simulations for an HETG/HRC-I setup with different focus positions. Without an offset, short wavelength photons, which get diffracted only by a small angle, are in focus. For larger offsets, photons at increasingly longer wavelength, i.e., those that get diffracted further away from the optical axis, are in focus. For example, the optimal spectral resolving power for the O_{VII} triplet (21.6 Å) is achieved at a focus position of ~+0.25 mm. However, the resolving power distributions are wide, so even with the flat HRC-I a large region of the dispersed HETG spectrum will still achieve a better resolving power than LETG observations.

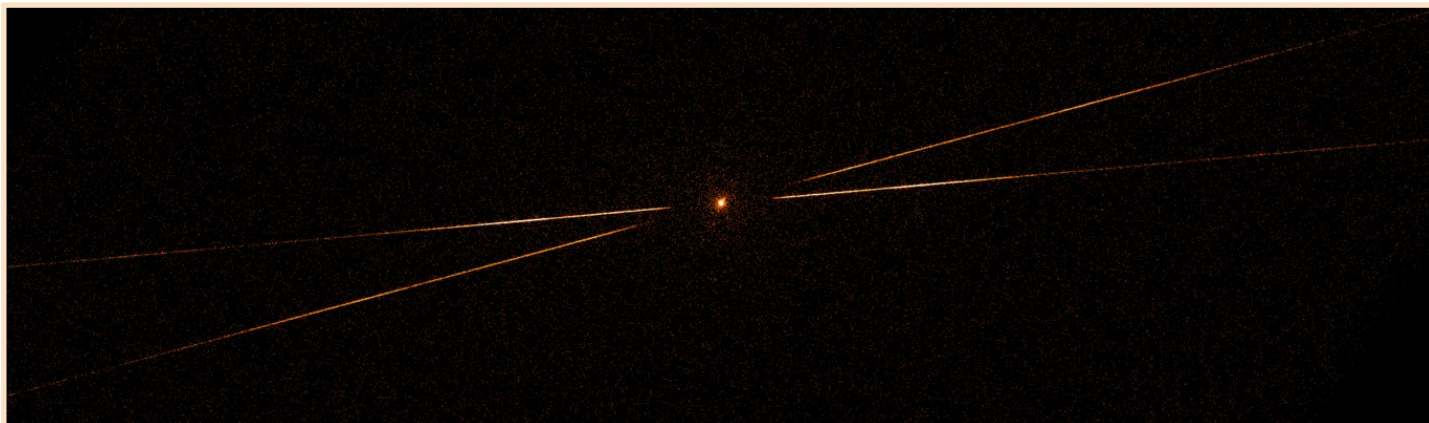


Figure 2: GX 3+1 (ObsID 13712) observed with HETG/HRC-I. The source is very bright and HEG and MEG arms can be seen easily on the detector image.

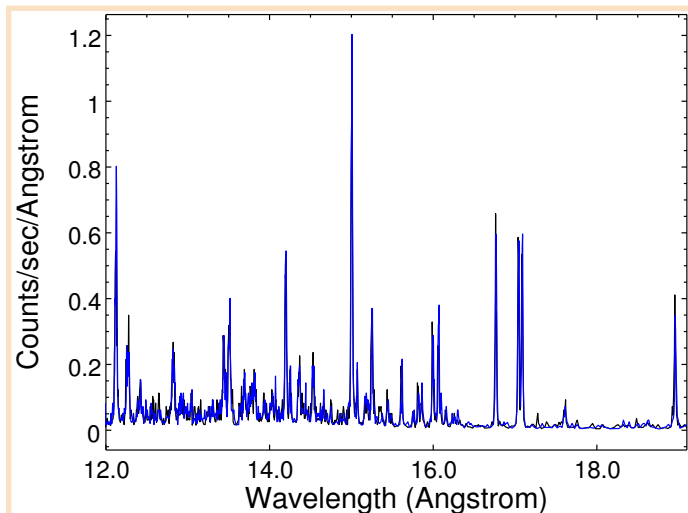


Figure 3: One section of the MEG Spectrum of Capella, observed with HETG/HRC-I. Black: negative orders. Blue: positive orders

Data from HETG/HRC-I Observations

So far, there are two HETG/HRC-I observations in the archive. The first one is ObsID 13712 (target GX 3+1, Figure 2). The object is a very bright continuum source and the HETG was used to reduce the count rate in zeroth order. The dispersed spectrum is visible on the detector, but of limited scientific use. The second observation (ObsID 19837) is from Capella, an active star and regularly observed calibration source, which was taken specifically to test the HETG/HRC-I mode (Figure 3). The position of the emission lines in the spectrum are well known, although their flux levels do change.

Presently, the processing of HETG/HRC-I observations is limited since the configuration is not yet fully supported, i.e., there are no CIAO threads to process the data and the required calibration products are not included in the CALDB. There is plenty of signal in the spectrum. Using a select sample of emission lines with little to no confusion, we can model the core of the HETG line spread function (LSF) with a simple Gaussian (http://space.mit.edu/CXC/LSF/LSF_0002/LSF_build2.html) to determine the resolving power and compare it to the values presented in Figure 1. This comparison is shown in Figure 4. As expected for a grating dispersed spectrum, the resolving power increases with wavelength and behavior in the observations is similar to that seen in Figure 1. Note that the O VII lines at 21.6 Å and 22.1 Å are not very bright and thus the uncertainties are large.

Does HETG/HRC-I Work?

The observation of Capella was a successful test of using the HETG with HRC-I. However, more work, specifically in the calibration and CIAO data analysis tools, is needed before this mode can be used routinely. At the current time,

this HETG/HRC-I configuration is only warranted for a few special cases where the LEG resolving power is insufficient but emission lines in the range 15–25 Å are crucial. On the other hand, with increasing contamination there will be more and more cases where the HRC can offer better overall performance than ACIS-S.

The Good News: What We Can Learn from Absorption

In this section, we highlight two recent scientific results that are based on absorption line spectroscopy using HETG data. The first example re-analyzes archival HETG observations to consider aspects of the data that were not central to the original observation. The data archive of existing HETG observations is quite rich and grows with every new cycle. The HETG instrument team tries to make it as easy as possible to view and retrieve archival data for example through the TGCat web-archive (<http://tgcate.mit.edu>). TGCat offers quicklook images of all reduced datasets and science-ready data products for download.

Fu et al. 2017 presented a new study of the bright Seyfert I galaxy NGC 3783. This target has accumulated more than 1 Ms of exposure time with *Chandra*/HETG and a number of previous publications have studied the spectral absorption lines to derive the properties of warm absorbers—with sometimes inconsistent results. The novelty of the Fu et al. (2017) study is the simultaneous fit of X-ray data from *Chandra*/HETG and UV data from *HST*/COS (both observations were taken within a few days of each other) to constrain the properties of the warm absorbers. Their simultaneous fit produces a model that requires a total of five warm absorbers. They report that only two of these seem to be in

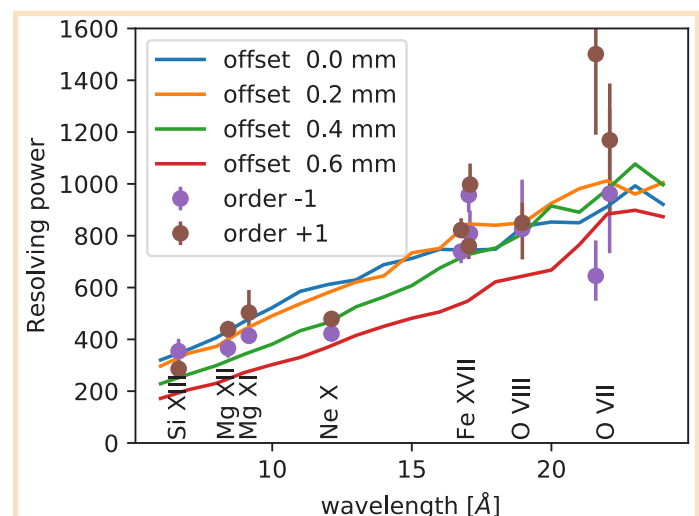


Figure 4: Predicted and observed resolving power for HETG/HRC-I observations. Capella was observed with a focus offset of +0.24 mm. Labels indicate which lines were used to measure the resolving power.

pressure balance, so that they can be described by a static model. A more detailed treatment is required to understand the remaining clouds. For example, two smaller clouds seem to have been blown out from the torus only very recently. The authors estimate a total mass outflow of 0.2–4 solar masses per year.

The second example of HETG absorption spectroscopy we highlight considered absorption between us and low-mass X-ray binaries (LMXB). Schulz et al. (2016) analyze HETG spectra towards several galactic LMXBs and in particular study the Si edge at 1.844 keV. There are several features near the Si edge which are caused by Si that is not free in atomic form, but where the energy of the edge is shifted because of ionization or because the Si is bound in dust grains. The edge feature is also measurably broadened due to the turbulent velocity of the gas by a few hundred km/s. The high turbulence and the ionization state indicate that most of the absorbing mass is located close to the LMXBs. In addition, Schulz et al. find that the edge structure can be variable on the time scale of days as the Si responds to changing ionization from the LMXB.

Summary

The HETG team is actively investigating observations with HETG/HRC-I. We hope that this combination can be useful for observers who want to use the HETG, but also require good signal between 15 and 25 Å. We have presented some promising preliminary work using this configuration, but note that this configuration is presently not supported for general observers. ■

References

- C. R. Canizares, J. E. Davis, D. Dewey, K. A. Flanagan, E. B. Galton, D. P. Huenemoerder, K. Ishibashi, T. H. Markert, H. L. Marshall, M. McGuirk, M. L. Schattenburg, N. S. Schulz, H. I. Smith, M. Wise. *The Chandra High-Energy Transmission Grating: Design, Fabrication, Ground Calibration, and 5 Years in Flight*. PSAP 117, 1144-1171 (2005).
- H. M. Günther, S. P. Matt, J. H. M. M. Schmitt, M. Güdel, Z.-Y. Li, D. M. Burton. *The disk-bearing young star IM Lupi. X-ray properties and limits on accretion*. A&A 519, A97 (2010).
- X.-D. Fu, S.-N. Zhang, W. Sun, S. Niu, L. Ji. *Joint fit of Warm Absorbers in COS and HETG spectra of NGC 3783*. Research in Astronomy and Astrophysics 17, 095 (2017).
- N. S. Schulz, L. Corrales, C. R. Canizares. *Si K Edge Structure and Variability in Galactic X-Ray Binaries*. ApJ 827, 49 (2016).

LETG Update

Jeremy Drake, for the LETG team

“If it ain’t broke...

don’t fix it.” Best said in a Northern English accent by a mature gentleman in a tweed jacket and a flat cap, holding a pipe by the bowl end and motioning the stem in the air for particular emphasis. A gentle poking gesture in the direction of the keen but naive youngster on the receiving end is also particularly effective. Yorkshire or Lancashire accents—hopefully not risking offence by conflating those two mortally-opposed bastions—sound best for the passing along of time-honored wisdom, giving the impression that wisdom must slowly seep out of other areas of the country, leading to foolish meddling with success in the Midlands, purely cosmetic “improvements” in Wessex, and needless “upgrades” in the Home Counties.

What a splendidly sensible maxim to live by though. And so, there we were, not fixing things that weren’t broken, but steadily going through our secret list of unsolved calibration problems—see *Newsletter 24* page 26 for a description of that sacred process—when the LETG phone, in its prime location on the desk, with the big red light on it, started to flash. It is our secure direct line to the *Chandra* Helpdesk, immune to the inevitable attempts at interference and hacking by hostile agents of foreign space missions. Cutting out the opaque cryptomission jargon, the gist of the communication was that someone had reported that our wavelengths were a little bit broken.

The LETG is much like a traditional transmission grating, where the diffraction pattern comprises a 0th order, corresponding to light passing straight through, and symmetric diffraction into higher orders either side, corresponding to

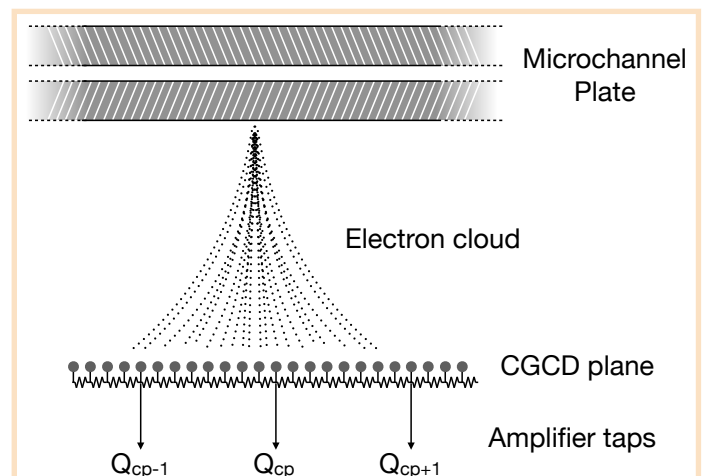


Figure 1: Schematic of the determination of photon event positions in the HRC detector. It is an analog instrument, and event positions are determined from the signals Q_{cp-1} , Q_{cp} , Q_{cp+1} from the nearest amplifier “taps” to a charge cloud from the bottom of the microchannel plate stack.

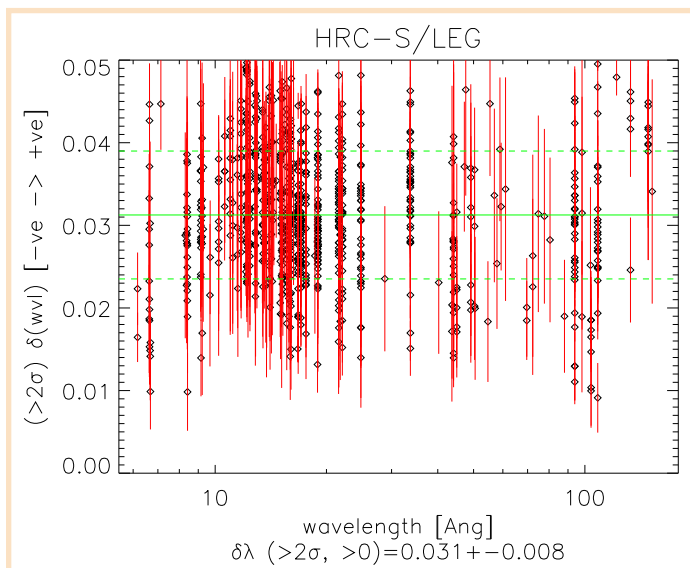


Figure 2: Measured shifts between lines seen in the $-$ and $+$ orders for a variety of strong lines in numerous LETG+HRC-S observations of coronal sources. Only lines detected at $>2\sigma$ and displaying a positive line shift are shown here, as diamonds with red vertical lines signifying $\pm 1\sigma$ error bars. The average line shift is represented by the horizontal green line, and $\pm 1\sigma$ width of the distribution of line shifts is shown as the horizontal dashed green lines. Figure courtesy of Vinay Kashyap.

“positive” and “negative” dispersion directions along the dispersion axis. In order to wring the most out of grating observations, both HETG and LETG, the positive and negative orders are either added together to combine the signal, or else analyzed together by simultaneous parameter estimation within a model fitting engine, such as *XSPEC* or *Sherpa*. The requirement for this of course is that the dispersion relation for $+$ and $-$ sides be identical, or at least to within the precision with which it is possible to measure it. This is quite easy if the detector is nicely physically pixelated, like a CCD. Diffracted photon positions can be assigned to particular pixels (or groups of pixels, nothing being quite so simple in the X-ray world) in which they were detected and that have precisely known positions in space.

The HRC-S detector does not have pixels though. Instead, the position of a photon event is determined from a charge cloud initiated by the photoelectric effect and boosted by a high voltage-fueled electron cascade within the capillaries of the microchannel plates. The charge cloud exiting the bottom of the plates—20 million or so electrons, or about one each for every Australian—is detected by a square grid of conductors connected to amplifiers, with the position being determined by the relative amplitudes of the signals seen in the nearest three amplifier “taps” in each orthogonal axis. Some charge spills outside of the three taps, which spoils the position determination algorithm; the resulting map of raw event positions has regular tap-spaced gaps, a bit like my dad’s wallpaper. The position spoiling depends on the shape of the charge cloud and, unlike my dad’s wall-

paper, can be corrected for empirically: hence the arcane term “degap correction” that is applied to close up the gaps.

That is not the end of the story though. *Chandra*’s fine point spread function demands sub-arcsecond precision in photon positions, of which the system is capable on paper. But it is an analog system and subject to little distortions and ripples, reminiscent of my dad’s wallpaper, that can perturb the position determination. Back in Newsletters 11 and 12, I described empirical corrections to the ripples along the dispersion axis using bright emission lines with accurately-known wavelengths. A source is typically dithered in a Lissajous pattern about 2 mm square, and the trails of bright lines on the detector nicely mapped out the distortions. Several years later, in the aimpoint region of the detector this was replaced by a more comprehensive job that utilized raster scans of point sources originally undertaken to monitor the detector point source imaging capability. The wallpaper was painted over: job done.

Which brings me back to the flashing red LETG phone. There are many suitable metaphors to describe X-ray mission calibration—one topic of *Newsletter 24*’s article. Perhaps the least unpleasant is the analogy of trying to squash a balloon between your hands: no matter how carefully you position your fingers or hold the balloon, as you squash down one or more pieces of it will blister through an inevitably unguarded fissure and pop out at you. Like a macroscopic perversion of Heisenberg’s Uncertainty Principle, something always seems to get in the way of calibrating multiple aspects of the system at once without repercussions in one or more of them. We had squashed down the balloon of photon position distortions, but had not noticed the little blister protruding from behind. By fixing the problem, we had also broken something.

The problem was that it was not possible to get truly continuous information on the photon position errors. At

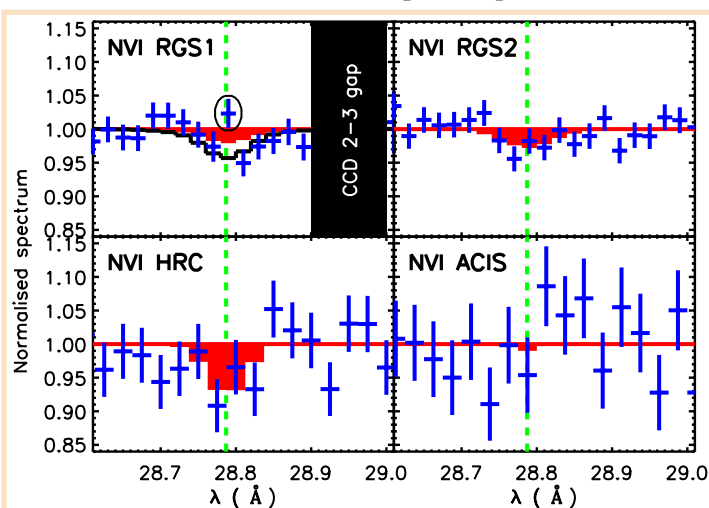


Figure 3: Normalized data (blue crosses) and best-fit models (solid red lines) of the transition temperature $N_{VI} \lambda 28.788$ line for RGS1 and RGS2 (upper panels), LETG/HRC-S (lower left), and LETG/ACIS-S (lower right). From Nevalainen et al. (2017).

some point, a bit like my dad's wallpaper, pasting together of corrections for different detector regions had to be done. Unappreciated at the time, this process apparently introduced about a 0.3" systematic position offset in the middle of the detector compared with regions further out, leading to small wavelength mismatches in + and - orders. Chief HRC calibration scientist and crack astrostastician, Vinay Kashyap, worked out the magnitude of the effect, illustrated in Figure 2. Vinay also concocted a correction for the problem in the form of a revised degap map that will be implemented and released by the time this Newsletter reaches your hands. The wallpaper has been repainted then. Subtle hints of the original pattern might still be discerned through the paint in a good light, just like at home. It is difficult to fix it further—more coats of paint in the form of extensive new calibration data would be needed. Besides, it is not really broken now.

Galactic Font of Wisdom

Though not from Lancashire or Yorkshire, Lyman Spitzer still had somewhat of a reputation for wisdom. In 1956, his paper "On a possible interstellar Galactic corona" proposed that neutral gas clouds far from the galactic plane were supported by a "rarefied, high-temperature gas" (Spitzer 1956). This idea eventually evolved into the "Galactic Fountain" of Shapiro & Field (1976), in which gas in the interstellar medium heated to a million degrees by supernova explosions expands vertically above the galactic plane, cools, and subsequently rains back down again. Observing this process provides insights into galactic evolution and the lifecycle of gas in galaxies.

The model predicts that there should, then, be infalling gas at "transition temperatures"—temperatures similar to that of the solar transition region, or 10^5 K or so. Such gas has in fact been detected in the far ultraviolet in ions such as O VI, N V, C IV, and Si IV (e.g., Wakker et al. 2012). While the 10^6 K coronal gas has been detected in X-rays, the transition temperature gas has not.

Nevalainen et al. (2017) have recently righted this wrong, by coadding about 3 million seconds of high-resolution grating observations of the blazar PKS 2155–304 obtained by the *Chandra* LETG and the *XMM-Newton* RGS. The blazar acts as a convenient backlight to shine through the galactic corona. And there it was, transition temperature gas revealed by the absorption lines of C VI, N VI (Figure 3), O V and O VI. Combining the X-ray data with FUV detections indicated that the gas is not photoionized. Instead, the authors found the oxygen line strengths to be in agreement with a model in which the observed ions originate in isobarically cooling gas with solar abundances and a temperature of $\log T(\text{K}) \sim 5.2$ and not far from collisional ionization equilibrium; all consistent with general expectations from the galactic fountain scheme.

Nothing broken worth fixing there then, either. ■

JJD thanks the LETG team for useful comments, information and discussion.

References

- Nevalainen, J., Wakker, B., Kaastra, J., Bonamente, M., Snowden, S., Paerels, F., & de Vries, C., 2017, *A&A*, 605, 47
 Shapiro, P. R., & Field, G. B. 1976, *ApJ*, 205, 762
 Spitzer, L. 1956, *ApJ*, 124, 20
 Wakker, B. P., Savage, B. D., Fox, A. J., Benjamin, R. A., & Shapiro, P. R. 2012, *ApJ*, 749, 157

Chandra-Related Meetings and Important Dates

Cycle 20 Peer Review:

June 18-22, 2018

Cycle 20 Cost Proposals Due:

September 27, 2018

Workshop: Accretion in Stellar Systems

August 8-10, 2018

Chandra Users' Committee Meeting:

Fall, 2018

Einstein Fellows Symposium:

Oct 2-3, 2018

Cycle 20 Call for Proposals:

December 2018

Brent Williams (1974–2017)



On the morning of Nov 8th, 2017, the CXC and MFSC teams were saddened by the news of the untimely passing of one of their most valuable members: Brent S. Williams. Brent's death came suddenly and unexpectedly, sending a ripple of heartache through the *Chandra* community.

Brent was an indispensable member of the Flight Operations Team (FOT), serving in a number of important positions along his path to becoming the Mission Planning Manager—a role that he not only thrived in, but one he seemed made for. His vast knowledge, diverse skill set, and affability made him an excellent planner. He was able to work extremely well under high-pressure situations, while also being a great leader, teacher, colleague, and friend.

Brent grew up in Fruitport, Michigan, with hundreds of tales to prove that he enjoyed all life there had to offer. Many of these stories involved his beloved wife, Joy, whom he married shortly after receiving his BSc in Chemistry at Hope College. Together, Brent and Joy moved to Boston in 1997, where Brent took a job as a cement chemist with Grace Construction Products. After a few years and a handful of patents, Brent made the life-changing decision to pivot from a career in chemistry to one in aerospace.

In 2000, Brent joined the *Chandra* team as a Command Controller, a job which involves being responsible for monitoring the health and safety of the spacecraft, commanding the spacecraft, maintaining the recorder, and first-line response to spacecraft anomalies. By 2002, he had shown a keen interest in science planning and accepted a position as a Mission Planner for the FOT, a role in which he excelled due to his creativity and problem-solving talents. During his time as a Mission Planner, he took on a myriad of additional tasks including flight dynamics, onboard clock correlation generation, and Deep Space Network resource

scheduling. He also assumed the mantle of FOT Training Manager, responsible for the new and recurring training of every FOT member. Brent accomplished all this while earning a Master's Degree in Engineering Management from Tufts University.

In 2008, having been recognized for his leadership skills, Brent was promoted to FOT Mission Planning Manager and spent the next ten years sculpting new approaches to planning that directly resulted in massive gains in efficiency, a significant reduction in planning error, and a quicker recovery to science following anomalous events. He chaired the Mission Planning Constraints Working Group, where he oversaw the development and modification of carefully crafted guidelines that positively impacted observing capabilities. He

presented this “During my first anomaly work in a poster session at the SpaceOps 2012 Conference in Stockholm, Sweden. While continuing to manage the Mission Planning team, Brent also became the FOT Operations Manager, acquiring a new set of responsibilities now tied to the immediate response of the spacecraft. He integrated his two teams seamlessly, creating a knowledge overlap that contributed to a better understanding of spacecraft planning and operations. For the next several years, he led both teams through multiple anomalies and large projects with passion, focus, and confidence.”

—John Scott, Lead Mission Planner

Brent's contributions to the mission have had long-lasting benefits. He was instrumental in the design and testing involved with Science-Only Safing Actions (SOSA), a project which saw a significant shift in onboard commanding with crucial benefits, in particular maintaining the spacecraft thermal and momentum states within safe limits after high-radiation stoppages. During and after a thruster anomaly, Brent led the planning team through a difficult period in which planning constraints were significantly tightened. Most recently, Brent spent two years overseeing the design and development of a new software process that not only expedited the building of command loads (especially for fast TOOs), but greatly improved error handling. As was usual for Brent, he was involved in a great many

aspects of the mission and his impact will continue to the mission's end.

Beyond his talents as a manager and engineer, Brent was foremost a people person. His vast knowledge, experience, and background meant that he could talk about anything and everything to anyone, and combined with his humility, quick wit, and charm, Brent made every moment special and intriguing. He always found a way to make even the most demanding moments endurable.

Brent was a great leader, manager, chemist, and engineer. He was an amazing colleague and friend, with good humor and a flair for storytelling. Above all, he was a wonderful husband and father. His wife Joy and their sons Fisher and Ruben are infinitely proud of him, as are we all.

Brent burned hot and bright for too short a time, and while his passing was devastating, he leaves fond memories and a lasting impact in his wake. We will miss you, B-Dub. ■

Prepared by John Scott

Chandra Calibration Update

Larry David

The ACIS detector gain continues to be calibrated in six month intervals by co-adding observations of the ACIS external calibration source (ECS) to increase integration time. ACIS is exposed to the ECS whenever it is in the stowed position, which occurs during each radiation belt passage. The six month intervals, as opposed to three month intervals used prior to 2016, are necessitated by the declining flux of the ECS (a radioactive ^{55}Fe source with a half life of 2.7 years). Since the ACIS gain continues to decline by about 0.1–0.2% per six month interval, the gain is still being calibrated to within the requirement of 0.3%. At the present time, the ACIS gain can still be calibrated on the same spatial scale as before (16" by 16" regions), but it will become necessary within the next few years to increase the region over which the gain is calibrated. The calibration team has also completed studies of astronomical sources (e.g., Cas A and the Perseus cluster) for use as potential gain calibration targets once the ECS flux has faded even further.

Gain calibration only requires the measurement of line centroids, while quantum efficiency (QE) calibration requires the measurement of the total flux in a line, which requires considerably better photon statistics. Previously, QE maps were released every two years. Due to the fading of the ECS, the next set of ACIS QE maps, which are currently under development, will cover a four year interval.

The calibration team continues to monitor the build-up of molecular contamination onto the ACIS optical block-

ing filters through imaging observations of the rich cluster of galaxies Abell 1795 and the oxygen-rich supernova remnant E0102-72 and gratings observations of the blazar Mkn 421. These observations are designed to track the time-dependence of the condensation rate onto the ACIS filter, the chemical composition of the contaminant, and the spatial distribution of the contaminant on the ACIS filters. Abell 1795 is observed semi-annually at the ACIS-I and ACIS-S aim-points. In addition, a more extensive raster scan of Abell 1795 on ACIS-I and ACIS-S is performed annually to map out the spatial distribution of the contaminant. A set of LETG/ACIS-S observations of Mkn 421 are carried out semi-annually in "Big Dither" mode (i.e., with a large enough dither to cover approximately one-fourth of the ACIS-S array). All observations acquired during 2017 are consistent with the present version of the ACIS contamination model in the CALDB, which was released in December 2016. Based on the full set of Abell 1795 observation acquired since launch, the rms scatter in the 0.5–2.0 keV flux is less than 3% when analyzed with the CALDB version of the ACIS contamination model.

Both the HRC-I and HRC-S have undergone a continuous decline in detector gain since launch. In addition, the HRC-S has also shown a continuous QE decline. These effects are corrected by the calibration team with annual updates to the HRC-I and HRC-S detector gains and the HRC-S QE. CIAO default processing automatically corrects for the time-dependent gain and QE losses to HRC-S data and time-dependent gain losses to HRC-I data. Due to the continued QE and gain decline, the operating high voltage of the HRC-S was increased in 2012 to restore the gain and QE to near launch values. However, since 2012, the gain and QE of the HRC-S has declined even faster. The calibration team has increased the cadence of the HRC gain and QE monitoring observations to four month intervals. At present, the HRC-S QE is declining by about 2–3% per year. While the HRC-I QE was stable over most of the mission, periodic observation of HZ43, for which most of the flux is below the C-K edge, show that the low energy HRC-I QE has declined by about 10% since launch. The calibration team is presently developing a time-dependent HRC-I QE file that will correct this problem. There are currently no plans to further increase the HRC-S high voltage, since the last increase produced an acceleration in the gain decline and any adjustment to the high voltage involves some risk to the detector. The calibration team will continue to release updates to the QE and gain files and the HRC-I and HRC-S effective area files used by PIMMS prior to each cycle. ■

Chandra Source Catalog

Ian Evans, for the
Chandra Source Catalog team

Release 2.0 of the *Chandra* Source Catalog (CSC) includes tabulated properties and FITS format data products for almost 375,000 source detections associated with more than 315,000 distinct X-ray sources on the sky. The detections were extracted from more than 10,000 *Chandra* ACIS and HRC-I imaging observations that were released publicly through the end of 2014. Multiple observations of the same field (defined as pointings that are co-located within 60 arcsec and obtained using the same instrument) are co-added, or “stacked,” prior to source detection, to maximize detectability of sources. Stacked-observation exposures range from 1.4 ks to 5.8 Ms, with a median exposure of 14.3 ks. Compared to release 1.1, an improved source detection approach allows detection of point sources reliably down to roughly 5 net counts on-axis, for exposures shorter than roughly 15 ks (for longer exposures, background becomes increasingly important, raising the limit on detectable net counts). The sky coverage of CSC release 2.0, totaling ~ 560 deg², is shown in Figure 1.

CSC release 2.0 includes information on roughly 100 tabulated properties for each identified X-ray source, as well as for the individual source detections on both the stacked and individual observations. They include positions and position errors, significance, spatial extent, multi-band aperture photometry (total and net counts, count rates, photon and energy fluxes, and model-dependent fluxes calculated using several common spectral models), hardness ratios, multiple spectral model fits, and inter- and intra-ob-

servations temporal variability. All numeric properties have associated uncertainties, usually independent lower and upper confidence limits. Furthermore, most properties are evaluated in 5 energy bands (ultrasoft: 0.2–0.5 keV, soft: 0.5–1.2 keV, medium: 1.2–2.0 keV, hard: 2.0–7.0 keV, and broad: 0.5–7.0 keV) for ACIS, and 1 energy band (wide: ~ 0.1 –10.0 keV) for HRC-I. As a result of this multiplicity, the catalog includes approximately 1700 columns of information, split across several tables. A sample of the key tabulated properties are shown in Figure 2.

In addition to the tabulated properties, the catalog includes roughly 40 different types of science-ready FITS data products totaling some 25 million files (~ 32 TB). The science-ready data products include merged detection lists, detection region event lists, exposure maps, responses, spectra, light curves, aperture photometry probability density functions, position error Markov chain Monte-Carlo draws, aperture photometry, hardness ratios, and spectral model fits for each photometrically-homogeneous subset of observations of a source (grouped together by a Bayesian blocks variability analysis), and limiting sensitivity maps.

This last year has seen significant progress towards completing release 2.0 of the CSC. At the time of writing the final *source properties* phase of processing is about 60% complete, meaning ~ 2 months processing remains to complete the catalog.

An updated preliminary detections list (*CSC 2.0 pd2*) that included detections from all of the 7,287 observation stacks that will appear in the final catalog was published in September 2017. The preliminary detections list includes position, likelihood, and intensity estimates (the latter is a proxy for aperture photometry), together with associated confidence intervals, for each detection. The release of *CSC 2.0 pd2* marked the end of the major *source detection* phase of processing for CSC release 2.0.

Following the *source detection* phase, detections from overlapping stacked observations that include the same location on the sky were cross-matched in the *master match* phase of processing to identify distinct X-ray sources on the sky. This step is necessary because the size of the *Chandra* PSF is a strong function of off-axis angle, and a single off-axis detection may be resolved into multiple sources in overlapping on-axis observations. A pre-release source list (*CSC 2.0 pre1*) that included CSC 2.0 source names following IAU standard nomenclature and identified the detections from

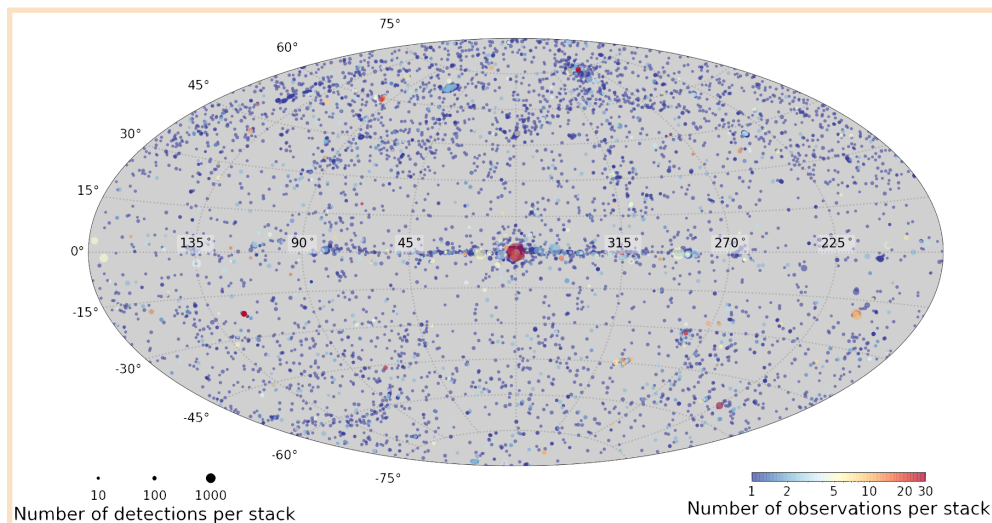


Figure 1. The sky coverage of CSC release 2.0, in Galactic coordinates. Each marker identifies the location of an observation stack on the sky. The size of the marker is proportional to the number of detections identified in the observation stack. The marker is color coded based on the number of observations that are co-added to construct the stacked-observation.

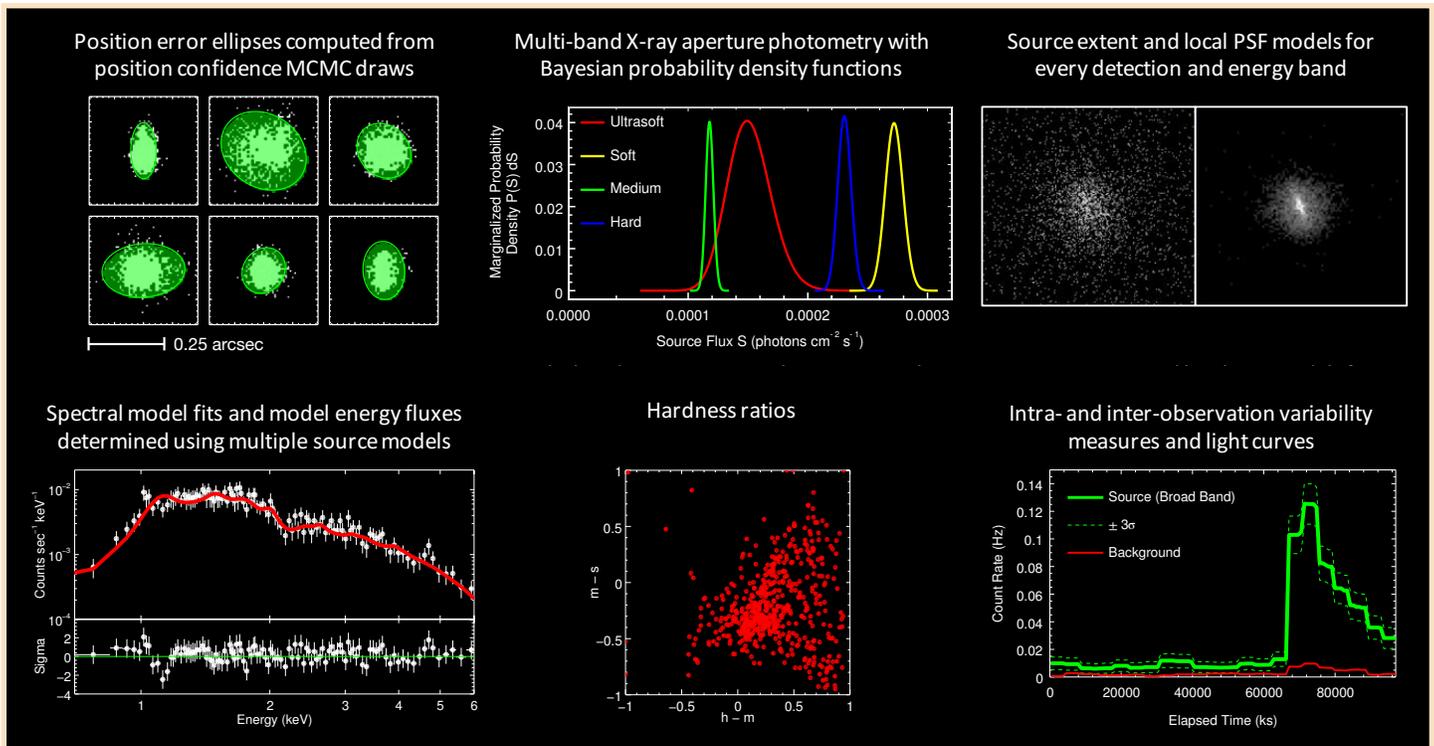


Figure 2. Examples of key source and detection properties that are included in CSC release 2.0. All numeric properties have associated independent lower and upper confidence limits, and most properties are evaluated in 5 energy bands for ACIS, 1 for HRC-I.

CSC 2.0 pd2 associated with each source, was published in mid-November 2017. The source names in the pre-release source list will not change in the final catalog release.

Both the *CSC 2.0 pd2* preliminary detections list and the *CSC 2.0 pre1* pre-release source list can be accessed through the CSC release 2.0 web site.

The *source properties* phase computes a detailed set of properties for each detection and source, generates limiting sensitivity maps, and populates the catalog databases. This processing phase is currently underway. The results of this phase are being made available to the community through the *CSCView* catalog interface. This allows users to see the tabulated properties and FITS format data products through the *CSCView* “current database” view as soon as processing completes for each overlapping group of stacked observations.

Once this last processing phase completes there will be a brief full catalog quality assurance review, after which the catalog will be frozen and the official CSC release 2.0 will be made available through multiple catalog user interfaces. The quality assurance review *could* result in the rejection of a very small (<0.1%) fraction of the detections identified in the *CSC 2.0 pd2* preliminary detections list and the *CSC 2.0 pre1* pre-release source list. The final CSC 2.0 release is expected around the end of the 1st quarter of 2018 and will be announced through multiple outlets.

Data access and documentation for CSC release 2.0 is available through the release 2 web site (<http://cxc.cfa.harvard.edu/csc2/>). The documentation describes the content

and organization of the catalog in detail and lists important caveats and limitations that should be reviewed prior to using the catalog data. Updates and news about release 2.0 will continue to be added to the website through the end of production. The current (release 1.1) version of the catalog may be accessed through the release 1 website site (<http://cxc.cfa.harvard.edu/csc/>), and this version will continue to be available indefinitely. ■

From *Chandra* to *Lynx*: A Summary of the Conference

Laura Lopez and Scott Wolk

A few weeks after the eighteenth anniversary of *Chandra*'s launch, the workshop “From *Chandra* to *Lynx*: Taking the Sharpest X-ray Vision Fainter and Farther” was held at Harvard University in Cambridge, MA, from August 8–10, 2017. Over one hundred astronomers attended the meeting, and the program included fourteen invited and twenty-nine contributed talks along with twenty-one poster presentations. The workshop spanned virtually all topics in X-ray astronomy, from supermassive black holes to objects in our Solar System and everything in between. *Chandra* has revolutionized our understanding of the high-energy Universe, and *Lynx*'s improved sensitivity and spectral resolution will enable substantial breakthrough progress beyond *Chandra*.

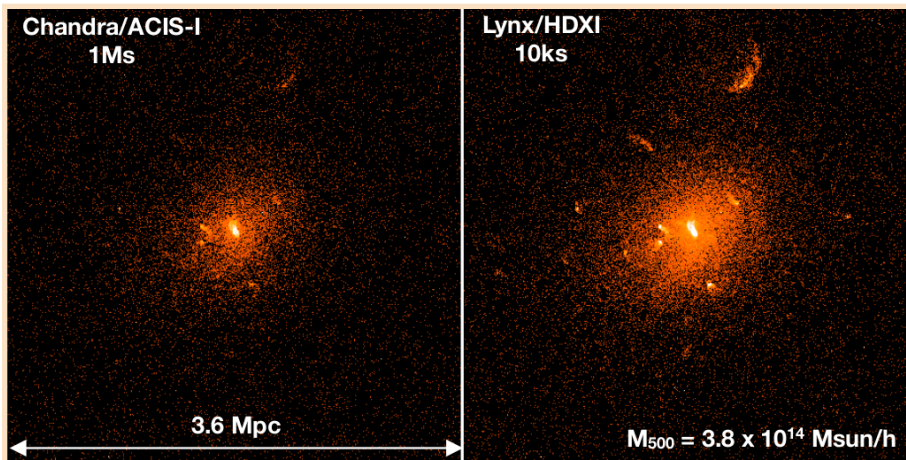


Figure 1: Figure from Camille Avestruz's presentation at the workshop comparing the *Chandra* (left) versus *Lynx* (right) view of a simulated galaxy cluster from the Omega500 simulation run at Yale University. Mock map generated by Erwin Lau using *pyxsim* and *SOXS* packages developed at SAO. The tremendous effective area of *Lynx* would allow it to readily detect the extended diffuse gas and faint point sources in a much shorter observation than *Chandra*. Additionally, *Lynx* has a relatively higher effective area in the soft X-ray band making it more sensitive to the soft X-ray emission coming from fainter substructures.

Belinda Wilkes opened the meeting with remarks on the status of *Chandra* (it is doing great!), and Alexey Vikhlinin followed with a summary of the progress on the *Lynx* mission concept study. The invited speakers at the symposium included Steve Allen, Niel Brandt, Joel Bregman, Lia Corrales, Bret Lehmer, Laura Lopez, Helen Russell, Nancy Brickhouse, Jeff Linsky, Laura Brenneman, Megan Donahue, Mike McDonald, Francesca Civano, and Benny Trakhtenbrot. They were asked to discuss the strengths and limitations of *Chandra* and to identify the *Lynx* capabilities that would be necessary to advance their fields. Many presentations emphasized the importance of high spatial resolution (at or better than *Chandra*) to limit source confusion in deep or crowded fields and to identify multiwavelength counterparts. The need for large effective area ($\sim 50 \times$ *Chandra*) and low background was also a common refrain. The greater throughput of *Lynx* would enable it to detect faint sources in tens of kiloseconds, whereas *Chandra* would require many

megaseconds to achieve the same sensitivities. For example, Figure 1 shows a simulated image of a galaxy cluster observed for 1 Ms with *Chandra* (left) and for 10 ks with *Lynx* (right).

Presentations and discussions at the *Chandra* to *Lynx* conference helped to refine two well-established *Lynx* pillars and motivated a third pillar on Galactic and stellar science. The *Lynx* Science and Technology Definition Team (STDT) has now identified three major science pillars that define the optics and instrument requirements: 1) the invisible drivers of galaxy formation and evolution; 2) the dawn of black holes; and 3) the energetic side of stellar evolution and stellar ecosystems.

The first pillar, *The Invisible Drivers of Galaxy Formation and Evolution*, broadly ties to many active areas of extragalactic science, including active galactic nuclei (AGNs), galaxy clusters, the hot circumgalactic medium (CGM), and numerical cosmology. The workshop speakers gave excellent presentations across these subfields, emphasizing the importance of understanding the cycle of baryons into, within, and out of galaxies as well as the role of AGN and stellar feedback in galaxy evolution. With *Lynx*, hot gas in galactic halos and cosmic web filaments will be observable in emission with imaging and in absorption with spectroscopy. X-rays are especially suited to investigate the met-

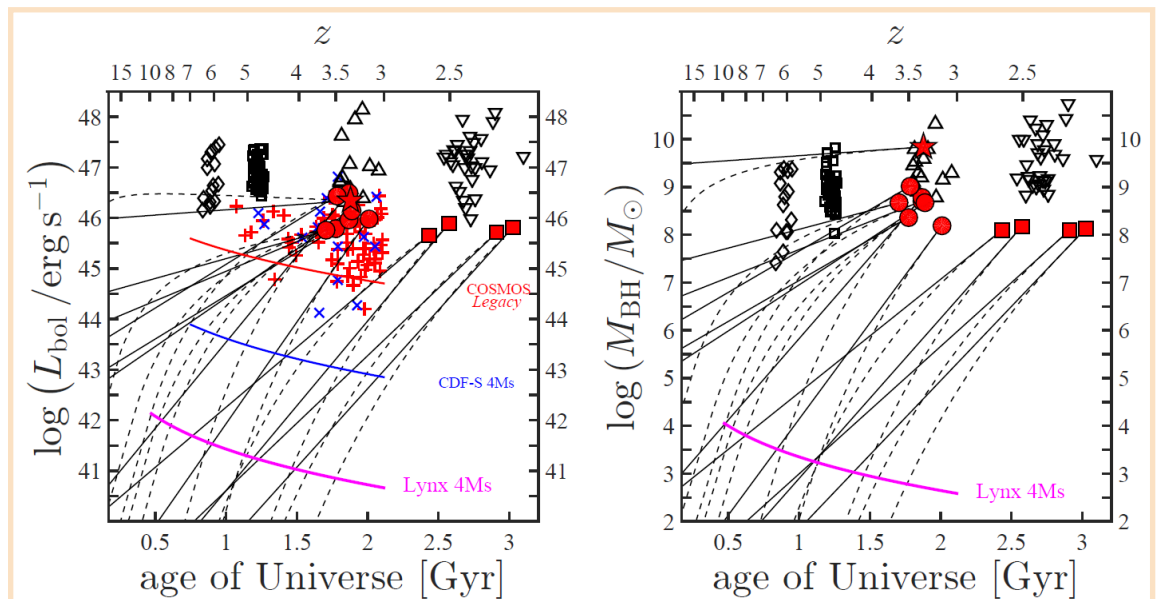


Figure 2: Figure from Benny Trakhtenbrot's presentation showing the limits on bolometric luminosity L_{bol} (left) and the corresponding Black Hole mass (right) that *Lynx* will be able to achieve. With 4 Ms of observation, *Lynx* will be able to detect the faint/low-M counterparts of the highest-redshift, high-mass luminous quasars, and trace the progenitors of high-redshift SMBHs.

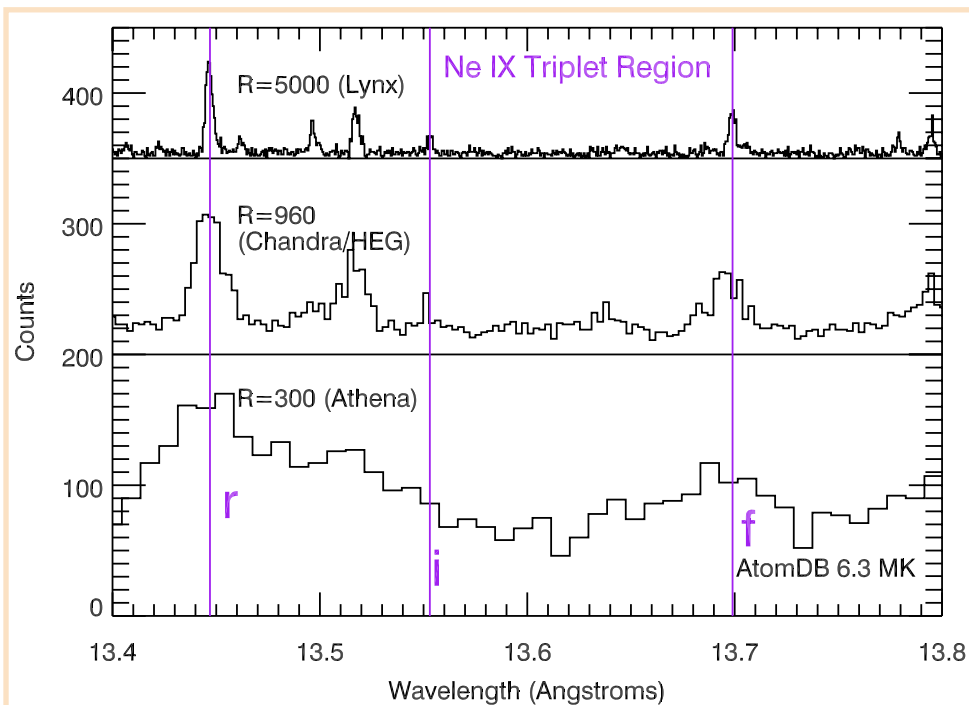


Figure 3: Figure from Nancy Brickhouse’s presentation at the workshop comparing the spectral resolution for density and temperature sensitive lines among *Lynx* (top), *Chandra* (middle) and Athena (bottom). The Ne IX triplet feature is critical to measuring coronal conditions, including accretion rates in young stars. With *Chandra*, this experiment has been performed on only a couple of stars. With gratings, the tremendous effective area of *Lynx* would allow it to observe this feature in dozens of stars in a single, short observation.

als of the CGM as e.g., $\sim 80\%$ of oxygen there is observable as O VII or O VIII at 0.5–0.7 keV. To make significant advancements, programs to study hot halos of galaxies require high-resolution spectra ($R \sim 5000$) of background AGN, the ability to detect low surface brightness, soft X-rays, and $R \sim 2000$ spectroscopy of extended objects on arcsecond scales.

The second pillar, *The Dawn of Black Holes*, is focused on the mystery of the origin of supermassive black holes (SMBHs). *Chandra* and *XMM-Newton* data have led to significant progress in our understanding of SMBHs, such as enlarging the sample of known X-ray selected AGN at $z \approx 4\text{--}7$. With *Lynx*’s planned sensitivity (of $\sim 10^{-19}$ erg cm $^{-2}$ s $^{-1}$), obscured and/or faint AGN populations at $z \approx 5\text{--}10$ will become accessible (see Figure 2). *Lynx* is predicted to detect $\sim 10^3$ SMBH seeds at $z \sim 8\text{--}10$ of mass $M \approx 3 \times 10^4 M_{\odot}$ in a 1 deg 2 field. Furthermore, *Lynx* will be able to trace the growth of these seeds and their co-evolution with host galaxies. Aside from low background and high throughput necessary to find high- z SMBHs, sub-arcsecond spatial resolution (both on- and off-axis) is also crucial to limit source confusion.

The design requirement to enable the first two pillars will allow for tremendous advances in understanding *The Energetic Side of Stellar Evolution and Stellar Ecosystems*. This third pillar covers a range of galactic science, from stellar

birth to death and beyond. Several speakers discussed how high-resolution imaging will allow unique science on star-forming clusters where each star imaged will have $R \sim 500$ spectra generated. The 50-year baseline of high-resolution imaging from *Chandra* and *Lynx* will also enable measurement of proper motions of most Galactic center X-ray sources with velocities > 100 km s $^{-1}$. The resultant low background (relative to the other X-ray missions flying in the 2030s) will allow deeper surveys. Soft X-ray sensitivity will be crucial to probe the most abundant metals in the Universe (e.g., oxygen). The inclusion of dispersive gratings will enable measurement of physics as diverse as the multi-phase interstellar medium and the details of coronal structure. The separate cross-dispersed spectra of multiple sources in a field enable breathtaking multiplexing capabilities—perhaps 100 high quality spectra, with 5 times HETG resolution,

in a single (< 1 day) exposure (see Figure 3)!

The meeting ended with a lively discussion about the path from *Chandra* to *Lynx*. Part of this discussion included a suggestion of a special call for proposals which could be viewed as testbeds of *Lynx* science. Following receipt and review of 29 white papers on candidate *Lynx* Pathfinder science, the *Chandra* Director’s Office released a call for *Chandra* observing proposals to carry out pathfinder science for a potential *Chandra* successor mission (CSM). Up to 1 Ms of *Chandra* Director’s discretionary observing time will be made available through the CSM call for proposals. 27 proposals requesting a total of 9.49 Ms were received by the 24 January deadline. The review panel met on the 14th of February at SAO. The results were announced and can be found at http://cxc.harvard.edu/target_lists/cycle19/csm_cyc19.html. ■

All of the presentations from the workshop are available online at <http://cxc.harvard.edu/cdo/cxo2lynx2017>.

CIAO in India

Antonella Fruscione, for the CIAO team

“The Chandra X-ray Center (CXC) offers a series of workshops aimed at helping users to work with the Chandra Interactive Analysis of Observations (CIAO) software.[...]”

If you are planning your own CIAO workshop and would like to request support from the CXC, please submit the relevant details to the Helpdesk. Proposals will be considered on a case-by-case basis.”

This is the statement on the [CXC CIAO workshop page](#). And this is what led Dr. Dharam Vir Lal, from the [National Centre for Radio Astrophysics](#) in Pune (India) to contact the CXC requesting help to organize a CIAO workshop at his institution.

Dr. Lal is himself an alumnus of one of the first CIAO workshops at the CfA. A few months and several logistical hurdles later, four CXC scientists left for India where forty students were eagerly awaiting to learn all about *Chandra*, X-ray astronomy and how to perform data analysis using CIAO. A group of CXC members in Cambridge was ready to support the workshop remotely, both with talks and support during the hands-on sessions, despite the ten-and-a-half hour time difference between Cambridge and Pune. The workshop lasted five days from the 23rd to the 27th of October 2017 and was hosted by the National Centre for Radio Astrophysics of the Tata Institute for Fundamental Research (NCRA-TIFR). The days were filled with talks (given on site and remotely from Cambridge), food, hands-on sessions, food and, did I mention, food?

The workshop was mainly aimed at students and postdocs new to X-ray and *Chandra* data. Talks covered a broad range of topics from an introduction to *Chandra*, X-ray data analysis, *Chandra* calibration, and CIAO, to more specific talks about X-ray imaging, spectroscopy, timing, statistics, modeling and fitting. The [full program](#) shows the breath of subjects that were covered. The majority of the participants were graduate students and postdocs coming from all over India, with the addition of a few local radio astronomers—NCRA is home to the Giant Metrewave Radio Telescope—interested in learning more about the X-ray band to complement their own radio data. All the students showed themselves to be extremely interested and engaged and, except for a small fraction who already had some experience with X-ray data analysis and had their own data to work on, followed a set of propaedeutic exercises aiming at teaching the basics of X-ray data analysis with CIAO.

As is often the case during CIAO workshops, the learning process was not unidirectional; watching the students learn and search for information, and interact with the soft-



Figure 1: Workshop students came from all corners of India.

ware, always provides insight for the CIAO team on where improvements are needed in terms of documentation and tools. It is so easy to believe that everything in the documentation is spelled out in the clearest way until a beginner tries to follow the instructions! Furthermore, by being physically present at the institute in India, we learned first hand just how much laptop setups can vary and how the absence of infrastructure that we take for granted (large bandwidth, latest and greatest laptops, uniform operating systems) can make using our software and documentation difficult. The experience highlights the need for software that addresses such environments. To overcome some of the connectivity problems the CIAO team brought the entire *Chandra* archive on a portable hard drive—all the X-ray photons detected by *Chandra* fit in less than 4Tb!—plus we had all the tar files needed for CIAO and CALDB installation on several flash drives, and we pointed the students to tools like `download_obsid_caldb` which performs a partial download of the *Chandra* Calibration Database (CALDB) and only downloads the files required for the analysis of a specific observation (OBSID). This tool tries to overcome the fact that the file size of the *Chandra* CALDB has become prohibitive for certain users on slow internet connections and those with limited free disk space. We also made use of the capability to download the entire CIAO website on a local laptop as explained in the [Download the CIAO website](#) thread.

The workshop logistics were entirely organized by NCRA-TIFR who did a fantastic job advertising the workshop all over India, inviting students whom they knew would be



Figure 2: Workshop participants. See http://cxc.cfa.harvard.edu/ciao/workshop/oct17_pune/ for complete workshop information.

particularly interested (for example because of their involvement with the Indian X-ray mission *ASTROSAT*) and selecting students from the many applicants. The workshop had no registration fee and all the students were provided room and board and some reimbursement toward travel expenses. Dr. Vir Lal of course took care of us from the time we landed in India to the time we left!

On the last day a “feedback session” was held between Dr. Vir Lal and the students (no CIAO team present!). The feedback for the CIAO team was extremely positive with the only request being the wish that the workshop were longer with more hands-on time and more in depth coverage of some subjects (e.g., psf simulation, Sherpa 2D modeling, timing).

Here is an excerpt of some of the most rewarding comments:

Did the participants get enough help/support during hands-on sessions?

Yes! In fact much more than what they asked for. It did not matter if the question was stupid or sensible, the CIAO people answered everything that was asked, they were not in a hurry and answered with patience.

Would you recommend this workshop to your friends/colleagues?

Yes! In fact one participant even shared that a colleague of his would also have benefited by coming. All said they would share the workshop website, their experiences with friends and colleagues in their home institution.

What about the CIAO documentation?

They found whatsoever they were looking for easily as well!

Maybe more examples on gallery (ciao/sherpa/chips) would be helpful.

Any general comment?

Everyone appreciated this effort! A complete new workshop, which was never conducted earlier. They especially appreciated the efforts of Nick [Lee] and Kenny [Glotfelty], who stayed awake at odd hours, fixed typos immediately, kept the workshop website updated with presentations, fixed issues pertaining to CIAO installations on Linux and anything else which was asked of them.

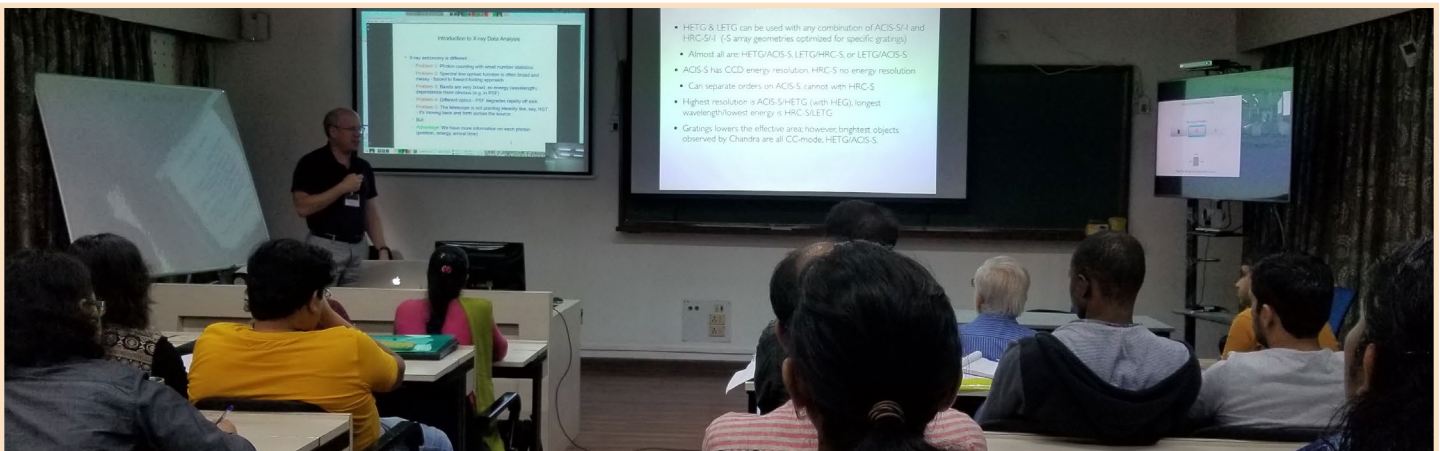


Figure 3: Workshop in progress

The Einstein Postdoctoral Fellowship Program: Morphing and Merging

Paul J. Green

A Brief History

In 1998, the year before *Chandra* (née AXAF) was to be launched, the *Chandra* Fellowship program began. Previous NASA mission-related postdoctoral fellowships had provided clear evidence for the value of such programs, to ensure that promising young scientists would keep pushing the boundaries of science, enhancing the return on the public's investment in these missions.

Each year, 5 new *Chandra* postdoctoral fellows were selected from about a factor of 10 to 20 more applicants from around the world, to undertake independent research broadly related to the scientific mission of the *Chandra* Observatory at a U.S. host institution for up to three years. To foster geographic and scientific diversity, no more than one new fellow per year could settle at a given host. The *Chandra* Fellowship was administered at the CXC by Nancy Ramage Evans for a decade. Most of the early *Chandra* Fellows are now faculty doing active research relevant to *Chandra*, and have spawned a generation or two of academic descendants who continue to enliven and enlighten the field.

Then, in 2009, NASA decided to merge the *Chandra* and Fermi (née GLAST) fellowship programs, together with a number of additional fellowships, into a combined program called the Einstein Fellowship. The Einstein Fellowship has sponsored from 10–12 new fellows each year, encompassing research areas related to the science goals of the Physics of the Cosmos program and its missions – high energy astrophysics, cosmological investigations relevant to Planck, WFIRST, or new dark energy missions, and gravitational astrophysics. Andrea Prestwich ran the Einstein Fellowship at CXC from 2010 until 2014, when I began to manage the program.

Fellows have gathered to share the results of their research at an annual symposium, every year since 1999. Each symposium has been both exciting and collegial, and the graphics have evolved from displaying scatter plots on an overhead projector to high-definition videos of large scale structure formation, black hole mergers, and MHD accretion discs.

Information about current and prior Einstein and *Chandra* Fellows, including programs and presentations from their symposia can be found at <http://cxc.harvard.edu/fellows>.

A New Postdoctoral Pangaea

To rebalance NASA Science research and analysis (R&A) funds relative to fellowship funds, the NASA



Figure 4: Mike Nowak (MIT), Antonella Fruscione, Rodolfo Montez, Vinay Kashyap (SAO) ready for the workshop banquet

From Dr. Lal

“Many many thanks to the Chandra X-ray Center teams of CfA and MIT to conduct an excellent Chandra/CIAO workshop at the NCRA-TIFR. We at NCRA-TIFR thank you and your team members for taking time to help and provide support, more importantly your patience and perseverance to conduct and to make this workshop a successful one. The participants have really appreciated the efforts and they have (hopefully, at least they claim so!) learnt a great deal and hence the future looks bright!”

Word is spreading about this first off-site *Chandra* workshop. Where is CIAO going to land next? ■

Astrophysics Division has decided to merge and reduce its three major astrophysics fellowships, the Einstein, *Hubble* and Sagan programs. Recently, these three programs have sponsored a total of about 30–35 fellows, but this will contract to 24 starting with the class of 2018.

Also starting this year, the application, selection and grants administration for fellows will be through STScI, and the three original categories will be combined under the umbrella of the NASA *Hubble* Fellowship Program (NHFP). The NHFP covers all of NASA astrophysics, with science themes preserved, broadly reflecting these questions:

- How does the Universe work?→NHFP Einstein Fellows
- How did we get here?→NHFP Hubble Fellows
- Are we alone?→NHFP Sagan Fellows

Salary and benefits remain at a similar level, competitive with other US prize fellowships. The 2018 NHFP Announcement of Opportunity was released September 1st 2017, yielding 350 complete applications by the deadline in early November.

Fifty panelists were recruited to participate in 6 topical science panels, reviewing a huge range of scientific research proposed by the applicants. At the selection panel meeting in Alexandria, VA during late January 2018, panelists faced the daunting task of ranking many impressive applications. After the review, we immediately began making offers to the top-ranked candidates. Offerees juggled their options and host institutions (with the new rule allowing a maximum of 2 new fellows per year at a single institution, and 5 total over any 3 year period starting 2018 or later). A NASA press release will announce the new 2018 class of 24 fellows in the Spring. Without any explicit linking to missions, the NHFP will encompass as broad a range of NASA astrophysics as ever.

Going forward, I will continue to supervise the NHFP Einstein Fellows, while Andy Fruchter and Dawn Gelino will shepherd the NHFP *Hubble* and Sagan Fellows, respectively. Kartik Sheth is the NASA Program Officer overseeing the NHFP. As we collaborate to develop the policies and procedures for running the merged NHFP program, during these shifts, we look forward both to continued spectacular scientific results from the fellows, and to the active input and participation of the entire NASA Astrophysics community.

The NHFP is headquartered on the web at <https://nhfp.stsci.edu>, which includes information on all the fellows. Any questions about the program can be addressed to nhfp@stsci.edu. ■

Visualizing and Using the Global *Chandra* Footprint

Raffaele D’Abrusco

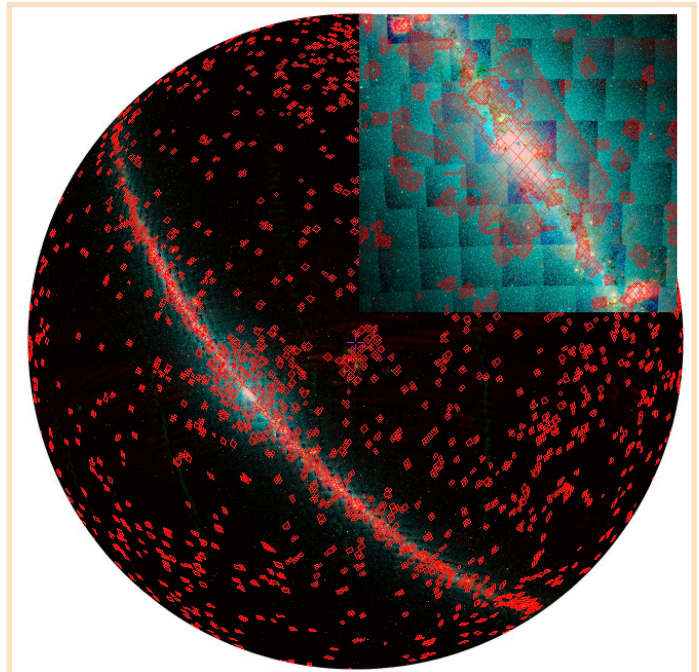


Figure 1: Visualization of the half-sky distribution of the footprints of all public *Chandra* observations (excluding gratings observations) with the CDA-generated MOC data product. The red tiles, which indicate the *Chandra* footprints, are overlaid on the HiPS color image of the WISE all sky survey. The inset in the upper right corner shows a magnified view of the center of the Milky Way.

With *Chandra* approaching its 20th year of operation, the total fraction of sky observed has reached the 1.9% mark. To the untrained eye, a map showing the footprints of all the public observations taken by *Chandra* would resemble a large and sparse collection of isolated rectangular shapes, a few islands of closely and orderly positioned tiles, and a patchwork of large, often connected regions, typically associated with structures in the sky, such as Sgr A* and the Andromeda galaxy.

A common question that astronomers ask is whether *Chandra* has observed a particular point in the sky. Based on the response, new projects involving observing proposals and/or the use of *Chandra* archival data, novel discoveries and innovative astrophysical insights may ensue. So, creating and distributing easy-to-use but powerful tools that answer this question is one of the key goals of the *Chandra* Data Archive (CDA).

Since November 2010, the CDA has offered access to the *Chandra* Footprint Service (FPS) (<http://exc.harvard.edu/cda/footprint/>), which provides users with information about *Chandra* observations within a given radius of a

position in the sky. The FPS provides visual access to chip geometry on the sky and tabulated instrumental and observational parameters of the available *Chandra* observations for the point in the sky. Nonetheless, the increasing interest in all sky population studies that require knowledge of whether very large number of sources are covered by *Chandra* observations, calls for new methods to visualize the *Chandra* footprint at a larger spatial scale and to quickly determine positions that are located within the footprint.

The need for this new visualization and analysis tool is being addressed by the CDA through the production of a new type of data product called Multi-Order Coverage maps (MOCs). MOCs combine the field-of-views of all public *Chandra* observations into a unique and conveniently compressed representation of the entire *Chandra* footprint. MOCs are optimized for interactive exploration at multiple levels of detail, i.e., spatial resolutions. The *Chandra* MOCs, in their FITS serialization, can also be used to filter a theoretically unlimited number of positions based on where they are located relative to the *Chandra* footprint. The MOC representation of astronomical footprints, which is recognized as a standard format by the International Virtual Observatory Alliance (IVOA), is based on the HEALPix tessellation and can encode arbitrarily complex geometrical shapes from the all sky level up to any desired spatial resolution based on the maximum value of the HEALPix level used to generate the MOC.

The MOCs of all *Chandra* observations that have become public by the end of 2017 are available from the CDA webpage (http://cxc.harvard.edu/cda/cda_moc.html). We also plan to start updating the *Chandra* MOCs on a weekly basis soon. The MOCs use HEALPix orders from 9 to 13, corresponding to average resolutions for the cells in the highest HEALPix level ranging from $\sim 6.8'$ to $\sim 25.7''$. The *Chandra* MOCs will also be discoverable across all VO-compatible data portals and interfaces. MOCs can be displayed in both local clients (Aladin; <http://aladin.u-strasbg.fr/>) and web-based applications, like ESAsky (<http://sky.esa.int/>). More importantly, *Chandra* MOCs can be used to select positions within the *Chandra* footprint, estimate global properties of the *Chandra* coverage (such as the total area covered), and compare the intersection of the *Chandra* footprint with footprints of other observations. These operations can be performed either via GUI tools such as TOPCAT and Aladin, or programmatically, using MOC-compatible libraries such as the Starlink Tables Infrastructure Library Tool Set (STILTS) or Python libraries MOCpy and PyMOC.

MOCs will complement the FPS by providing astronomers quick and comprehensive access to the geometric properties of *Chandra* observations, thus making the X-ray Universe seen by *Chandra* more easily discoverable and accessible. ■

Data-Driven VR/AR 3D Models: Walking Among the Stars

Kimberly Arcand and Kathy Lestition

In conjunction with scientists observing with *Chandra* and other telescopes, the Public Outreach program at the *Chandra* X-ray Center has pioneered two programs that enable scientists and the public to visualize dimensionally, touch, and even walk through astronomical sources.

Our initial example, Cassiopeia A (Cas A), was the first supernova remnant to be modeled in 3D based on observational data. In 2009, PI Tracy Delaney (then at MIT) analyzed data from *Chandra*, *Spitzer* and ground based telescopes. The data set was ported to unique brain imaging software that had been modified for use in astronomy by the Astronomical Medicine Project run at the CfA to create a 3D model. Initially the model was primarily accessible only in on-line video and via a special online video viewer developed by the Smithsonian to showcase its collections.

Since 2013 we have seen the rapid development and proliferation of 3D printers for mass use, and we worked with experts at the Smithsonian in Washington to convert the Cas A 3D files into a printable format. Cas A was not the easiest object to start with. The turbulent details of the explosion are difficult to print and the tendril-like jets have



Figure 1: Testing the Oculus Rift version of Cas A VR in the Brown YURT. Photo: E.Jiang



Figure 2: 3D prints of SN1987a (left) and Cas A (right). Photo: K. Arcand

a habit of breaking off, even with careful handling. Having failed to find a commercial printer willing to deal with the intricacy of the model, we have printed a limited number of copies using in-house 3D printers while we continue to search for a commercial option.

The models were used with great success over the summer at the National Federation for the Blind Youth Slam. Modifications suggested by the Youth Slam participants, such as sturdier jets and a version made in halves to provide access to the interior structure, have been implemented. See <http://chandra.si.edu/photo/2013/casa/> and <http://chandra.si.edu/deadstar/deadstar.html>.

Achieving success with a 3D printed Cas A sparked a search for other sources with 3D potential. The 30th anniversary of SN1987 A in 2017 offered such an opportunity. Based on models by Salvatore Orlando that were constrained by *Chandra* observations we developed a printable 3D model of the important threshold that SN 1987A has just passed: the shock wave moving beyond the dense ring of gas produced late in the life of the pre-supernova star and into the poorly known medium beyond. Orlando's visualization is based on a sophisticated 3D simulation that incorporates the complex interaction among radiation, matter and relativistic effects, reproducing the observed properties of the supernova. See <http://chandra.si.edu/deadstar/sn1987a.html>.

Also using simulations developed by Orlando, we have printed a 3D model of the latest outburst (2014) from the binary system V745 Sco. The printed model was made in two pieces to allow exploration of the shapes of the blast wave and the ejecta morphologies. See <http://chandra.si.edu/photo/2017/v745/> and <http://chandra.si.edu/deadstar/v745.html>.

The downloadable files and instructions for printing the three astronomical sources as well as a 3D *Chandra* spacecraft can be found at http://chandra.si.edu/resources/illustrations/3d_files.html.

We have used these models at AAS meetings and also with the public and at educational events. The physical representation of the astronomical data generates both interest and increased learning capacity in the public, and scientists report that it increases their understanding of the physical attributes of sources. We urge anyone with an interest in developing 3D models of astrophysical sources that they are working with to contact us to talk about what additional data or simulations would be necessary to turn that data into a physical representation. There is no single approach: each source has different requirements.

Simultaneously with the growth of 3D printing, software and hardware developments also spurred the dissemination of virtual reality (VR) and augmented reality (AR) into new content areas. VR is computer technology that simulates a user's physical presence in a virtual environment. AR adds elements, such as text, overlays, audio—essentially informational interactivity—to enhance that experience

with sensory input and additional information about the virtual environment.

We were excited by the technological advances in the VR and AR realms and realized that we could expand the applications of our 3D models. For example, instead of our telling people where and what to look at in Cas A, VR/AR lets people explore the object themselves by, for the first time, navigating through the physical representation of the real data from the remains of an exploded star. The Cas A 3D VR/AR project is a collaboration between the CXC and Brown University's Center for Computation and Visualization in Providence, RI, and provides opportunities for public communications, informal education, and research.

Additionally, the CXC has worked with the Smithsonian Learning Lab to broaden the reach of *Chandra*'s Cas A 3D model. We collaborated to create a browser-based interactive 3D application that includes a 360 degree video playable in YouTube and also compatible with VR viewers such as Google Cardboard. The application has related educational resources and activities that can be explored at <http://s.si.edu/cas-a>.

Chandra has repeatedly observed Cas A since the telescope was launched into space in 1999. Each exposure has added new and important data to the growing bank of information that astronomers use to study this object. This deep reservoir of data also allows astronomers and visualization specialists to take the Cas A data set far beyond the two-dimensional imagery that exists for most astronomical objects. The latest release of a two-dimensional Cas A image shows the locations of the various elements produced in the explosion. This information is incorporated into the interactive VR/AR activity with color-coding and labels for enhanced visual interpretation.

The 3D visualization and VR/AR also have scientific applications. The 3D visualization shows that there are two main components to this supernova remnant: a spherical component in the outer parts of the remnant and a flattened (disk-like) component in the inner region. The insight into the structure of Cas A gained from the 3D visualization is important for astronomers who build models of supernova explosions.

The VR project is being made available in an open access format suitable for VR caves as well as on the Oculus Rift platform. More information on Cas A in VR is available at <http://chandra.si.edu/vr> or one can contact Kimberly Arcand for more information about accessing those files (kkowal@cfa.harvard.edu). Additional data-driven 3D astronomical objects are also in the works for the *Chandra* VR/AR experience. Again, we strongly encourage any scientist who is interested in using their data in 3D or VR/AR experiences to contact Kimberly Arcand. ■

The Results of the Cycle 19 Peer Review

Andrea Prestwich

The programs approved for *Chandra*'s 19th observing cycle are now underway. The Cycle 20 Call for Proposals (CfP) was released on 14 December 2017 and the proposal deadline was 15 March 2018 but delayed by one day due to weather. Cycle 18 observations are nearing completion.

Cycle 19 Proposal Statistics

Cycle 19 proposal statistics can be found in Figures 1–7 and on the CXC website at: http://cxc.harvard.edu/target_lists/cycle19/cycle19_peer_results_stats.html

The distribution of science panels is shown in Table 1 and Joint Program statistics in Tables 2 and 3.

Cycle 19 included a call for Very Large Proposals (VLP), a category requiring > 1 Ms of observing time. VLPs were last solicited in Cycle 12. The total amount of time allocated in Cycle 19 was 16.7 Ms including 3.9 Ms to 7 approved LPs and 2.7 Ms to two VLPs. The overall oversubscription in observing time was 5.8, slightly higher than in the past few cycles (Figure 5). The increase in the oversubscription was driven primarily by an enthusiastic response to the VLP call. We received 15 VLPs requesting a total of 27.7 Ms. The oversubscription in time for VLPs was 10.2, compared to 5.9 for the LP oversubscription and 4.9 for the GO oversubscription.

The funding available for Archival proposals increased from \$1,050K in Cycle 18 to \$1,500K in Cycle 19. This one-time increase was possible because an unusually large number of TOO programs in recent years were not triggered. Funds allocated to these proposals were recycled

Table 1: Panel Organization for Cycle 19

Topical Panels	
Galactic:	
Panels 1,2	Normal Stars, WD, Planetary Systems and Misc
Panels 3,4	SN, SNR + Isolated NS
Panels 5,6	WD Binaries + CVs, BH and NS Binaries, Galaxies: Populations
Extragalactic	
Panels 7, 8, 9	Galaxies: Diffuse Emission, Clusters of Galaxies
Panels 10, 11, 12	AGN, Extragalactic Surveys
Big Project Panel	
BPP	Large and Very Large Proposals

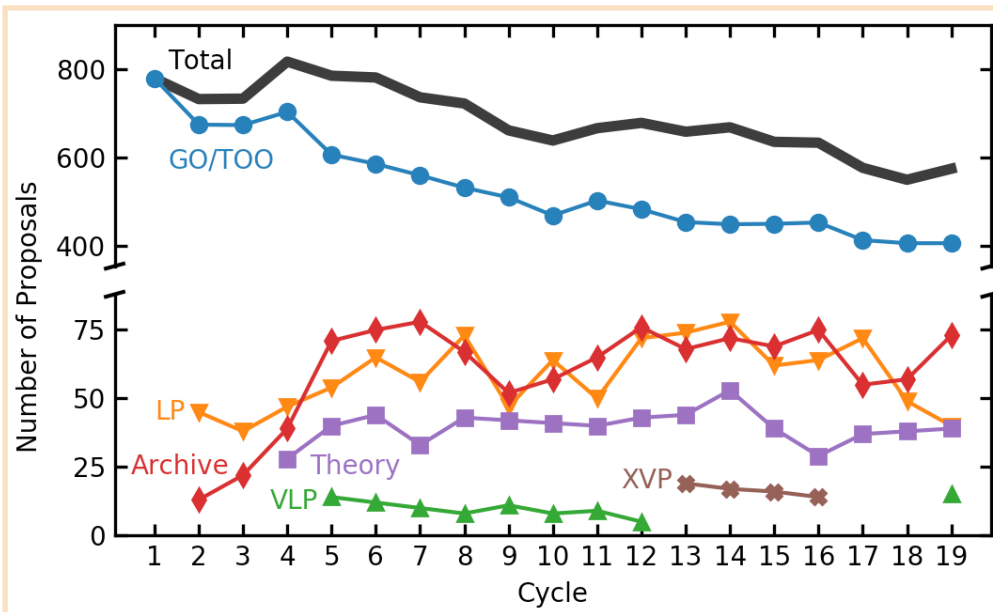


Figure 1: The number of proposals submitted in each proposal category (e.g., GO, LP, Archive etc.) as a function of cycle; note the vertical axis is broken at ~400 proposals to better show the individual proposal categories. Since more proposal categories have become available in each cycle, the number classified as GO has decreased as others increased. The total number of submitted proposals (solid black line) is remarkably constant.

into the Cycle 19 GO budget. The total number of submitted proposals increased in Cycle 19 relative to Cycle 18 (574 vs. 546). This upswing was due to an increase in the number of submitted Archival proposals (possibly motivated by increased available funding) and proposals submitted in response to the VLP call.

Plagiarism Screening

The CXC policy regarding plagiarism was clarified in the Cycle 19 CfP as follows:

“It is not acceptable to use plagiarized text in a *Chandra* proposal. Any material reproduced from another source must be contained within quotes and complete references given. Text that is “recycled” from papers authored by the PI or CoIs is acceptable in the context of a *Chandra* proposal” (Section 3.5 of the CfP).

The text of all submitted science justifications was screened using commercial plagiarism software (iThenticate). A handful of proposals had small amounts of text that appeared to be lifted from published sources and/or had incomplete references. Most of the flagged proposals contained text derived from one of the col’s publications, and these are not in violation of our policy. Some flagged proposals used a short phrase that was contained in multiple different source documents. In the few instances where there were slight violations along those lines, PIs were informed so they could correct the issues in future papers/proposals, and no further action was taken.

Timeline for Peer Review Results

Prior to Cycle 19, the approved target list was posted on the CXC website about 2 weeks after the Peer Review, and official emails sent to PIs (containing approved targets, Peer Review comments and budget allocations) later in the summer. In Cycle 19, NASA-HQ requested that we decrease the time between proposal submission and official notification of the results. In response to this request we split the notification emails into “accept/reject” and “budget”. The accept/reject emails were sent on 17 July 2017, one week after the target list was posted. The accept/reject emails for observing proposals contained approved targets and Peer Review comments. The accept/reject emails for archive and theory proposals contained

information on whether the proposal had been approved (yes or no) and Peer Review comments. Emails containing budget information for all proposals were sent on 7 August 2017. We anticipate sending separate accept/reject and budget emails for the foreseeable future.

Table 2: Time awarded by the Chandra Peer Review on other facilities

Observatory	# Accepted Proposals	Total Time
Hubble	7	37 orbits
NuStar	3	210 ks
NRAO	7	50.5 hours
Swift	3	157 ks
XMM-Newton	2	248 ks
NOAO	4	6.03 nights

Table 3: Chandra Time Awarded by other facilities

Observatory	# Accepted Proposals	Total Time
Hubble	4	254.0
XMM-Newton	1	22.0
NRAO	4	136.2

Cost Proposals

PIs of proposals with US collaborators were invited to submit Cost Proposals, due in Sept 2017 at SAO. Each project was allocated a budget based on the details of the observing program (see *CfP* Section 10.4). Awards were made at the allocated or requested budget levels, whichever was lower. The award letters were e-mailed in December, in time for the official start of Cycle 19 on 1 Jan 2018. ■

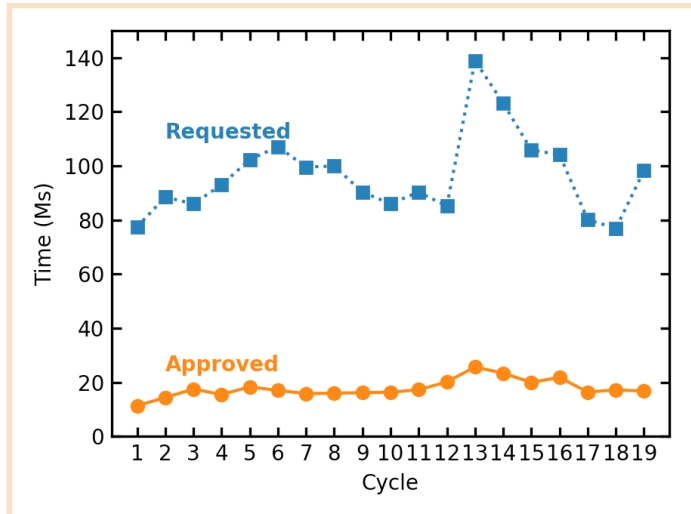


Figure 2: The requested and approved time as a function of cycle in Ms including allowance for the probability of triggering each TOO. The available time increased over the first three cycles, and in Cycle 5 with the introduction of Very Large Projects (VLPs). The subsequent increase in time to be awarded due to the increasing observing efficiency and the corresponding increase in requested time in response to the calls for X-ray Visionary Projects (XVPs) in Cycles 13-16 is clear.

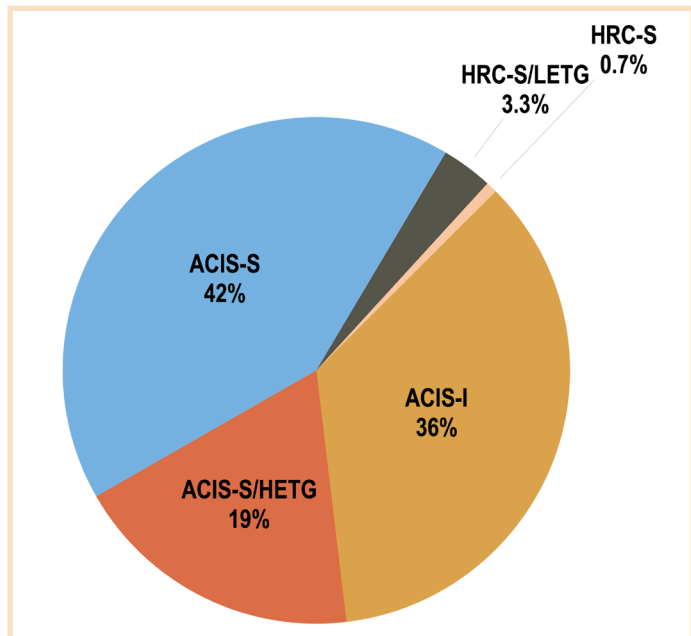


Figure 4: A pie chart showing the percentage of *Chandra* time allocated to observations for each instrument configuration.

Table 4: Requested and Approved Proposals by PI Country

Country	Requested		Approved	
	#Prop	Time	#Prop	Time
Argentina	1	50.00	1	50.00
Australia	1	61.00	1	61.00
Belgium	3	710.00	1	10.00
Bulgaria	1	40.00		
Canada	8	1921.00	1	170.00
Chile	2	120.00		
France	4	770.00	1	150.00
Germany	18	4202.00		
Greece	3	444.40		
Hungary	1	100.00		
India	4	350.00	1	30.00
Israel	1	450.00		
Italy	33	9188.00	7	639.00
Japan	11	2185.00		
Korea	1	80.00		
Mexico	2	670.00		
Netherlands	8	940.00	2	205.00
Poland	1	75.00	1	75.00
Russia	1	160.00		
Spain	6	1044.00		
Sweden	2	350.00		
Switzerland	1	350.00		
Taiwan	3	627.00		
Turkey	4	540.00		
UK	25	8425.00	9	3314.00
USA	429	67885.69	130	14126.00
Total Foreign	145	33852.40	25	4704.00

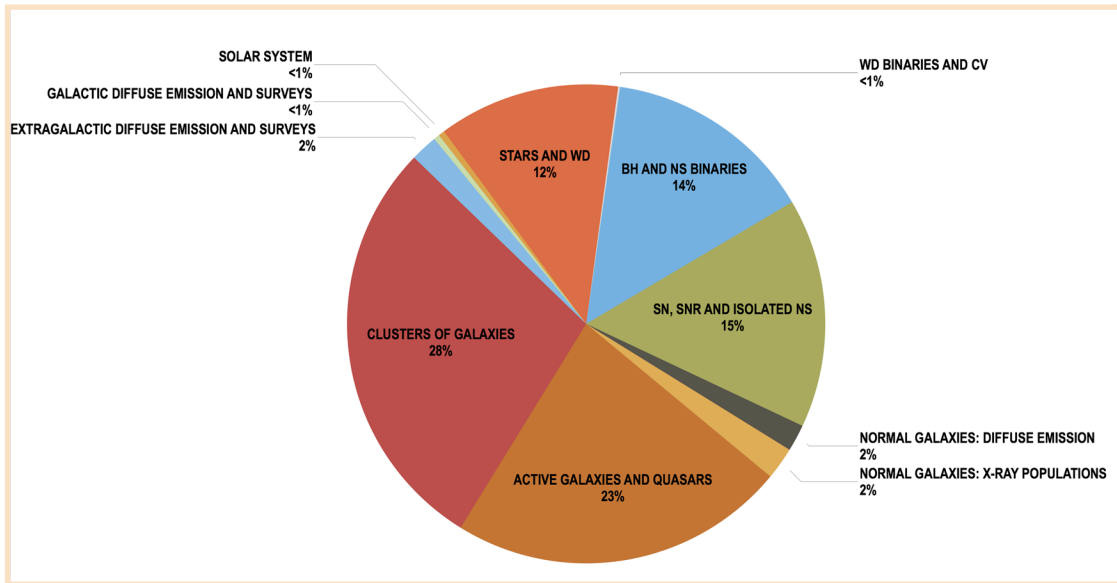


Figure 3: A pie chart indicating the percentage of Chandra time allocated in each science category. Note that the time available for each science category is determined by the demand.

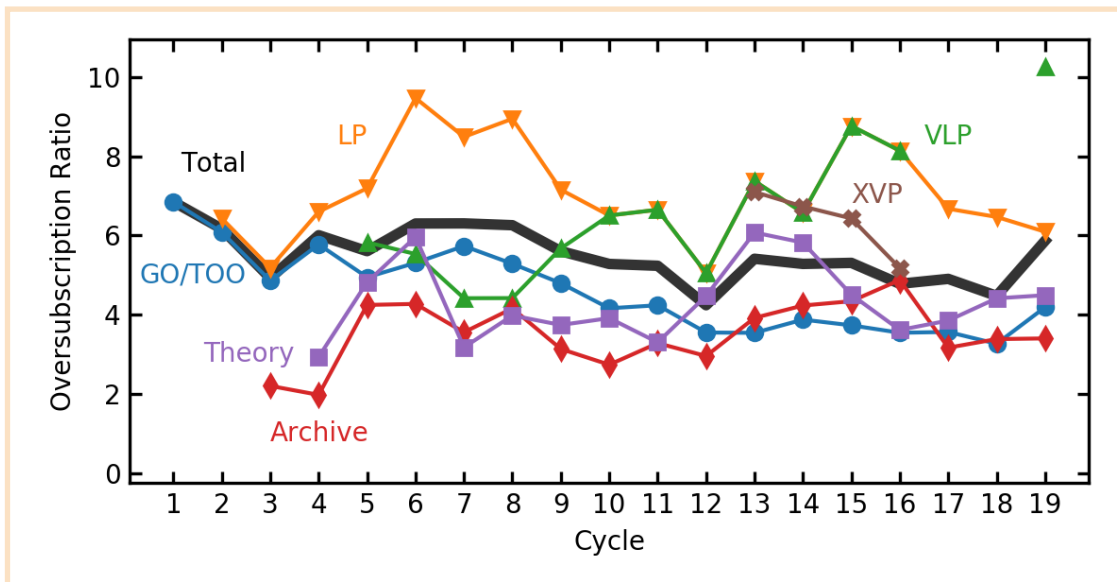


Figure 5: The effective oversubscription ratio in terms of observing time for each proposal category as a function of cycle. The total oversubscription numbers are remarkably constant. Note that some of the fluctuations are due to small number statistics (e.g., Theory proposals).

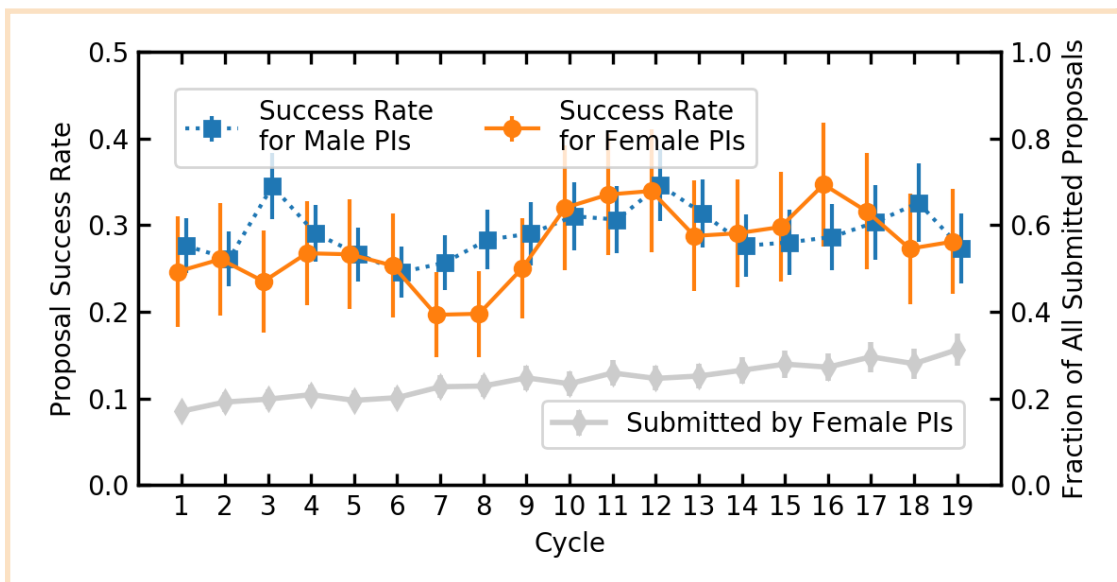


Figure 6: The success rate of male (blue squares) and female (orange circles) PIs as a function of cycle and the overall fraction of female PIs (grey diamonds). Since Cycle 10, the success rate for female and male PIs has been statistically indistinguishable.

2017 Press Releases

Megan Watzke

Date	PI	Object	Title
January 5, 2017	Niel Brandt (Penn State)	CDF-S	Deepest X-ray Image Ever Reveals Black Hole Treasure Trove
January 5, 2017	Reinout van Weeran (CfA)	Abell 3411 and Abell 3412	Astronomers Discover Powerful Cosmic Double Whammy
January 6, 2017	Dacheng Lin (U. New Hampshire)	XJ1500+0154	Black Hole Meal Sets Record for Length and Size
February 24, 2017	Salvatore Orlando (INAF)	SN 1987A	The Dawn of a New Era for Supernova 1987A
March 13, 2017	Arash Bahramian (Univ. of Alberta)	47 Tucanae X9	Star Discovered in Closest Known Orbit Around Likely Black Hole
March 29, 2017	CXC Director's Office		NASA Announces Astronomy and Astrophysics Fellows for 2017
March 30, 2017	Franz Bauer (Pontifical Catholic University)	CDF-S XT1	Mysterious Cosmic Explosion Puzzles Astronomers
May 2, 2017	Stephen Walker (GSFC)	Perseus Cluster	Scientists Find Giant Wave Rolling Through the Perseus Galaxy Cluster
May 31, 2017	Edwige Pezzulli (Univ. of Rome)	CDF-S	Early Black Holes May Have Grown in Fits and Spurts
September 6, 2017	Rachel Booth (Queen's University)	24 Sun-like stars	X-rays Reveal Temperament of Possible Planet-hosting Stars
October 3, 2017	Shobita Satyapal (George Mason Univ.)	5 pairs of merging SMBH	Scientists Find Elusive Giant Black Hole Pairs
October 16, 2017	Daryl Haggard (McGill), Raffaella Margutti (Northwestern), Eleonora Troja (GSFC)	GW 170817	NASA Missions Catch Light from a Gravitational-Wave Event
November 30, 2017	Trevor Dorn-Wallenstein (Univ. of Washington)	M31	Giant Black Hole Pair Photobombs Andromeda Galaxy
December 19, 2017	Joseph Conlon (Oxford Univ.)	Perseus Cluster	A New Twist in the Dark Matter Tale
December 29, 2017	Kim Arcand (CXC)	Cas A in 3D	A New Stellar 'Reality' Show Debuts

Links to all press releases can be found at: <http://chandra.harvard.edu/press/>

Additional image releases and other features that have been released are available at: <http://chandra.harvard.edu/photo/>

The *Chandra* Bibliography

Sherry Winkelman, for the CDA Team

As a member of the *Chandra* community, you may have noticed that Chaser provides links to publications which analyze *Chandra* data and that ADS provides links to *Chandra* data analyzed within a publication. If you have ever wondered where those links come from and how are they maintained, the answer is the *Chandra* Bibliography, which is curated and maintained by the *Chandra* Data Archive (CDA). Since September 2000, the CDA has been curating the *Chandra* Bibliography with two goals in mind: 1) aiding astronomers in their research by providing links between *Chandra* data and the literature on both ADS and Chaser and 2) provide tools to measure the science productivity of *Chandra* data in the astronomical literature.

The Metadata

The bibliography has four basic categories of *Chandra*-related publications: 1) *Chandra* Science Publications (CSP), where the *Chandra* data contributes significantly to the science presented within the publication; 2) *Chandra* Observatory Publications (CXO), for publications about *Chandra* instruments, software, or operations; 3) Miscellaneous *Chandra* Publications, when a publication refers to the *Chandra* observatory in some way but does not rise to the level of CSP or CXO publication; and 4) Not *Chandra* Related publications, for instances when ‘*Chandra*’ or ‘CXO’ is in the text of the publication, but the publication does not fit within any of the other categories. These categories provide the framework for the *Chandra* Bibliography.

In addition to these categories, we collect a rich set of metadata that describes the *Chandra* relation to a publication in greater detail. Some of the flags we include for each publication describe: data use, e.g., direct/indirect analysis, multi-observatory analysis, computational analysis; essential publisher information; data origin verification; location of the data, e.g., main text, table, figure; *Chandra* instruments and software; associated catalogs and surveys; additional observatories and wavebands; acknowledgment of data, tools, services, and grants. A simplified interface to the bibliographic database which provides simultaneous browsing of the archive and the literature can be found at <http://cxc.harvard.edu/cgi-gen/cda/bibliography>.

How are *Chandra* Data Being Used?

We took a look at trends related to: 1) direct analysis, which is data analysis that begins with *Chandra* data products provided by the CDA, versus indirect analysis, which is data analysis that uses published results that were based on *Chandra* observations and 2) multi-observatory analysis of data. Our trends are based on refereed CSPs from 2013 to the present because complete tagging is available only for this small interval. When looking at direct and indirect

data analysis in publications, we see that 20–30% of the refereed CSPs contain only analysis of the *Chandra* data provided by the CDA (direct analysis) and 15–30% contain only analysis based on previously published results (indirect analysis). The other 50–60% of refereed CSPs contain direct analysis of *Chandra* data combined with multi-observatory analysis, theory and/or computational analysis, or further analysis of previous results (direct + additional analysis). Of the CSPs with direct + additional analysis of data, 93% have a multi-observatory component in the analysis.

Which broad electromagnetic regions (or wavebands) and observatories are most often used in conjunction with *Chandra* data? When looking at these trends, we split the CSPs between those which focused on *Chandra* surveys and their catalogs and those which did not in order to see if there were any differences. When looking at how many wavebands *Chandra* data were combined with (X-ray from another observatory is considered another waveband here), we see no significant difference between CSPs using *Chandra* survey data and those without *Chandra* survey data. We do see some significant differences when we examine which observatory data are combined with *Chandra* data but there are no general trends. *Chandra* survey data were used with 34 other observatories, while non-survey data were used with 79. Not too surprisingly, *HST*, *Spitzer* and *XMM-Newton* were most often used with *Chandra* survey data and they are used with equal frequency (12.1%). On

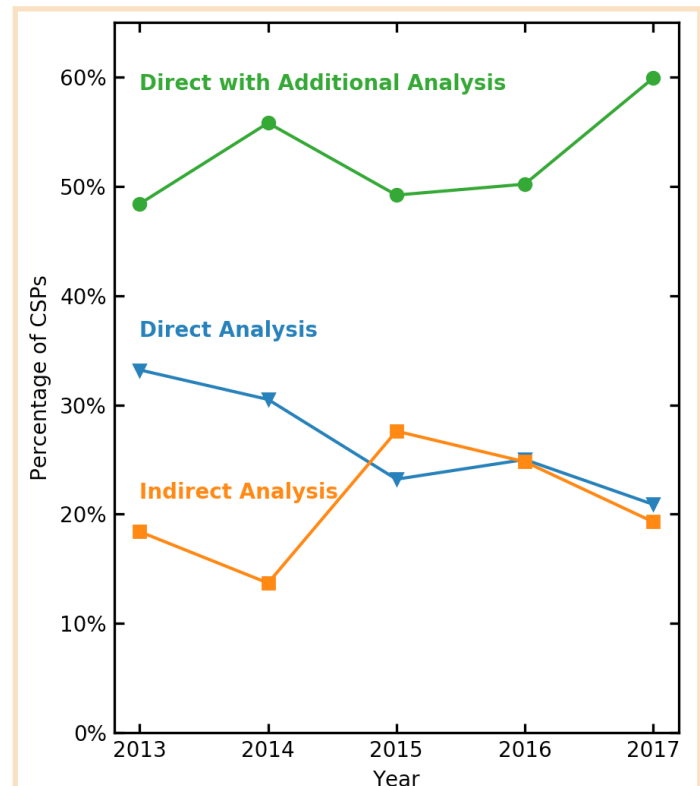


Figure 1: Percentage of CSPs with direct or indirect analysis of data.

the other hand, *XMM-Newton* (17.6%) was used most often with non-survey data with *HST* (9.1%) and *Swift* (8.5%) being used at about half the rate as *XMM-Newton*. The high rate of combined use of *XMM-Newton* and *Chandra* data is likely due to the complementary strengths of the two X-ray missions, while the combination of *Chandra* data with NASA’s other Great Observatories is possibly a consequence of the fact that they were designed to have matching spatial resolution to maximize the scientific return of the missions. To give a sense of the multi-observatory use of *Chandra* data in the literature we summarize the frequency of usage of 20 observatories’ data combined with survey and non-survey *Chandra* data.

We noticed an emerging trend in recent CSPs with regards to multi-observatory analysis: CSPs include a growing number of observatories. From 2013 to 2017, the fraction of CSPs that combine *Chandra* data with at least one other observatory has steadily grown. Amongst the CSPs that include data from at least one other observatory, the trend has been towards combining *Chandra* data with more and more observatories in a single CSP. Since 2014, the fraction of CSPs combining *Chandra* data with three or more other observatories has grown steadily while the fraction of CSPs combining *Chandra* data with only one other observatory has decreased. The rate of change from

Table 1: Multi-Observatory Usage of Chandra Data

Observatory	% with Survey Data	% with Non-Survey Data
<i>HST</i>	12.1	9.1
<i>Spitzer</i>	12.1	4.1
<i>XMM-Newton</i>	12.1	17.6
VLA	5.9	6.2
Herschel	5.2	1.2
Subaru	3.5	1.0
Keck	2.8	1.3
VLT	2.8	1.7
WISE	2.8	1.2
UKIRT	2.1	0.5
<i>NuStar</i>	1.7	4.6
<i>Swift</i>	1.4	8.5
ROSAT	1.4	1.1
Gemini	0.3	1.6
<i>Suzaku</i>	0.3	3.6
Fermi	0.0	1.6
GMRT	0.0	1.7
Integral	0.0	1.4

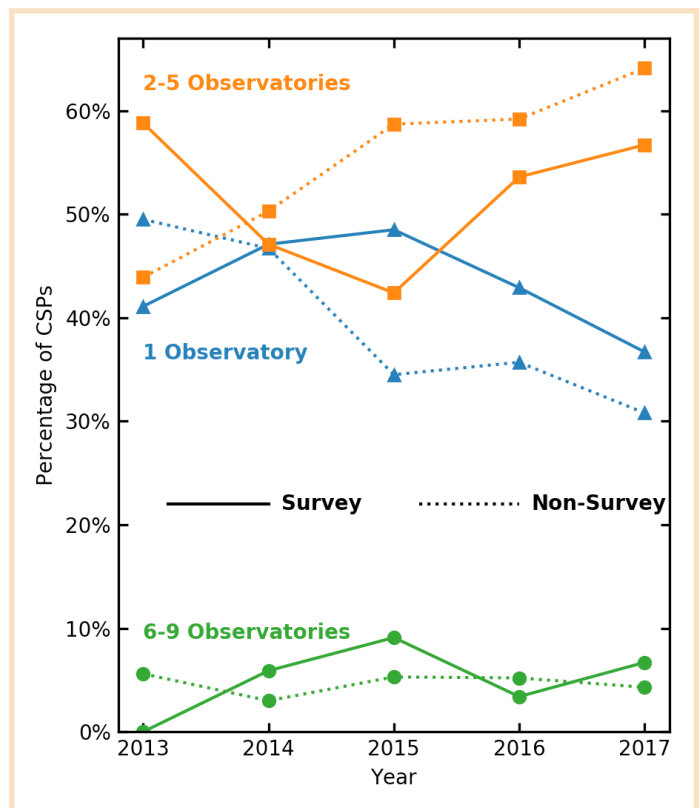


Figure 2: Percentage of CSPs using data from multiple observatories

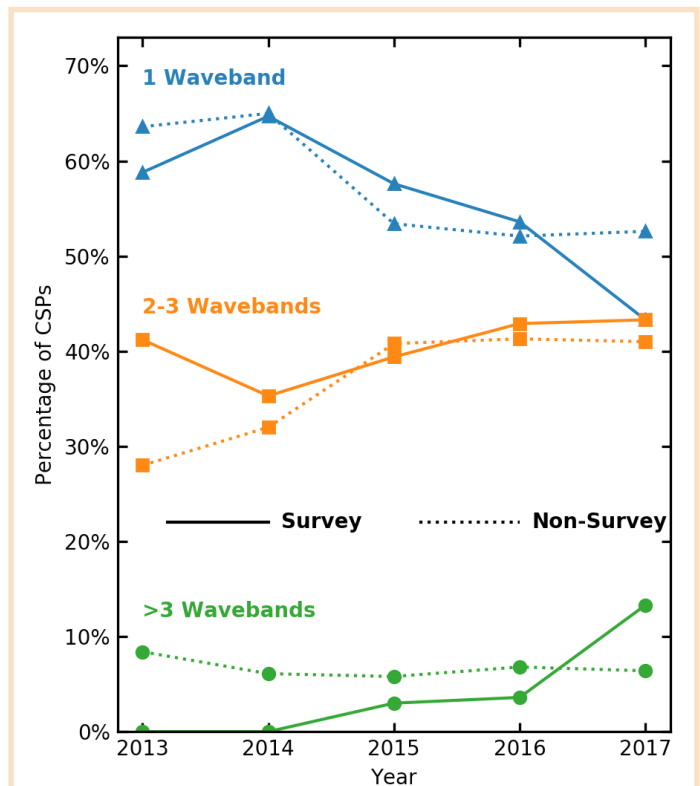


Figure 3: Percentage of CSPs using multiple waveband data.

one observatory to multiple observatories is greater for CSPs unrelated to *Chandra* surveys. We are also seeing an increase in CSPs that include data from five or more observatories, but it is too early to determine if this is a trend.

History and Effort

Such deep analysis of how *Chandra* data are used within the astronomy community is only possible by collecting a wide range of metadata. Over the years the metadata included in the *Chandra* Bibliography has undergone two major expansions. Each expansion in metadata was accompanied by new classification tools; added complexity to the bibliography database; and an intense backfill effort to bring the entire bibliography up to the new version. We have accomplished much with < 1 FTE for most of the mission. Major versions and their major advancements are listed below:

Version 1 (September 2000–June 2004) covered only full journal and proceeding articles with direct analysis of *Chandra* data and links to those data. The curation and dissemination of the bibliography were performed by a single person on a weekly basis.

Version 2 (April 2003–present) expanded the bibliography to include the four categories of *Chandra* publications we use today; covered abstracts and theses as well as all types of astronomical articles; data links were made for direct analysis of data only; and included minimal flags to describe the *Chandra* science context of CSPs. Curation and dissemination was now performed by two to three people and the backfill effort took about a year.

Version 3 (October 2013–present) included a vast expansion of metadata; data linking was extended to all CSPs, including those with indirect analysis of data; and curation was separated from dissemination. Curation is performed by two people, while dissemination is performed by a single person.

Due to the size of the bibliography and the complexity of the metadata and data linking in Version 3, the backfill efforts for this new version will be much greater than past expansions. We have complete metadata coverage for all four categories of publications from 2014 to present. All refereed CSPs from 1999–2000 and 2013 to present have complete metadata coverage, with completion of refereed CSPs from 2001 and 2002 expected by the end of June 2018.

The *Chandra* Bibliography has become an integral part of the CDA and is frequently used to assess the science output of the observatory. It has become a precious resource for management of the mission, demonstrating the necessity for gathering metadata for grants and acknowledgments as well as the use of *Chandra* tools. At the same time, long-term trends observed by curators have led to the addition of metadata describing the *Chandra* connection in publications, which suggest complex and interesting questions about the science impact of *Chandra*. And of course, we are always investigating new ways to present the metadata to the research community as well. ■

Useful Chandra Web Addresses

Chandra

<http://chandra.harvard.edu/>

CXC Science Support

<http://cxc.harvard.edu/>

Science Publication Guidelines

<http://cxc.harvard.edu/cdo/scipubs.html>

CIAO Software

<http://cxc.harvard.edu/ciao/>

Chandra Calibration

<http://cxc.harvard.edu/cal/>

ACIS: Penn State

<http://astro.psu.edu/astro-research/facilities/chandra>

High Resolution Camera

<http://cxc.cfa.harvard.edu/cal/Hrc/>

HETG: MIT

<http://space.mit.edu/HETG/>

LETG: MPE

<http://www.mpe.mpg.de/xray/wave/axaf/index.php>

LETG: SRON

<http://www.sron.nl/missions-astrophysics/chandra>

MSFC: Project Science

<http://wwwastro.msfc.nasa.gov/xray/axafps.html>

NASA's Chandra Page

https://www.nasa.gov/mission_pages/chandra/main/

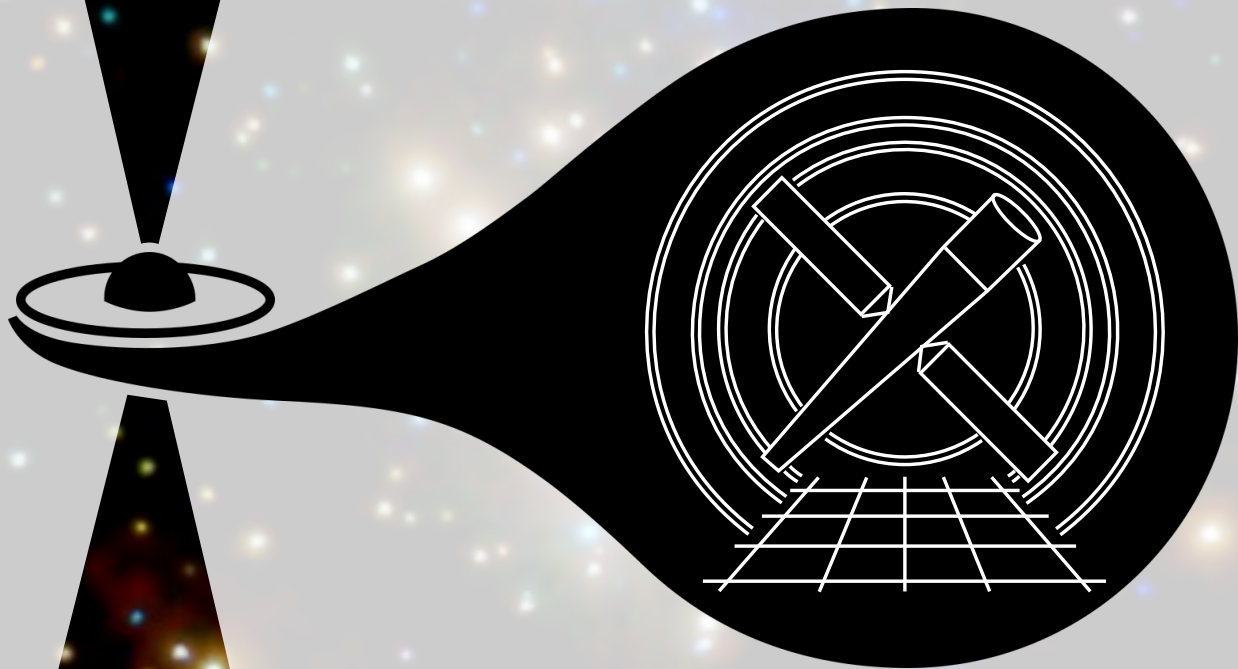
Chandra Users' Committee Membership List

The Users' Committee represents the larger astronomical community for the *Chandra* X-ray Center.

If you have concerns about *Chandra*, contact one of the members listed below.

Name	Organization	Email
Alicia Aarnio	University of Colorado	<i>Alicia.Aarnio@colorado.edu</i>
Tamara Bogdanovic	Georgia Tech	<i>tamarab@gatech.edu</i>
Ori Fox	Space Telescope Science Inst	<i>ofox@stsci.edu</i>
Dale Frail	NRAO	<i>dfrail@nrao.edu</i>
Elena Gallo	University of Michigan	<i>egallo@umich.edu</i>
Simona Giacintucci	NRL	<i>simona.giacintucci@nrl.navy.mil</i>
Nora Loiseau	ESA	<i>Nora.Loiseau@sciops.esa.int</i>
Thomas Maccarone (chair)	Texas Tech	<i>thomas.maccarone@ttu.edu</i>
John Mulchaey	Carnegie Observatories	<i>mulchaey@obs.carnegiescience.edu</i>
John Silverman	University of Tokyo	<i>john.silverman@ipmu.jp</i>
Dom Walton	CalTech	<i>dwalton@srl.caltech.edu</i>
Ex Officio, Non-Voting		
Jeff Hayes	NASA HQ	<i>jeffrey.hayes-1@nasa.gov</i>
Stefan Immler	NASA HQ	<i>stefan.m.immler@nasa.gov</i>
Wilt Sanders	NASA HQ	<i>wilton.t.sanders@nasa.gov</i>
Allyn Tennant	NASA/MSFC, Project Science	<i>allyn.tennant@msfc.nasa.gov</i>
Martin Weisskopf	NASA/MSFC, Project Scientist	<i>martin.c.weisskopf@nasa.gov</i>
CXC Coordinator		
Andrea Prestwich	CXC Director's Office	<i>aprestwich@cfa.harvard.edu</i>

CHANDRA SCIENCE WORKSHOP
ON
ACCRETION
IN
STELLAR SYSTEMS



AUGUST 8-10, 2018

CAMBRIDGE, MA USA

<http://cxc.harvard.edu/cdo/accr2018>

NASA MISSIONS CATCH FIRST LIGHT FROM A GRAVITATIONAL-WAVE EVENT

Astronomers have used NASA's Chandra X-ray Observatory to make the first X-ray detection of a gravitational wave source.

Chandra was one of multiple observatories to detect the aftermath of this gravitational wave event, the first to produce a detectable electromagnetic signal of any type. This discovery represents the beginning of a new era in astrophysics.

To read the complete image release, see <http://chandra.si.edu/photo/2017/2nstars/>.



Hubble: 22 Aug 2017



Chandra: 19 Aug 2017



Chandra: 26 Aug 2017



Published by the
Chandra X-ray Center